Highlights

Validation of the STEG code using experiments on Two-Phase flow across horizontal tube bundles

Shixian Liu,Fei Yin,V.I. Melikhov,O.I. Melikhov

- The results of the validation of the STEG code are presented.

- Experimental data obtained on two steam generator (SG) models are used.

- The void fractions and water velocities are measured in different locations.

- 90% of experimental points are predicted by the STEG code with an accuracy of 10%.

Validation of the STEG code using experiments on Two-Phase flow across horizontal tube bundles

Shixian Liu[a,b], Fei Yin[a], V.I. Melikhov[a,c,*] and O.I. Melikhov[a,c]

[a]*National Research University "Moscow Power Engineering Institute", Krasnokazarmennaya 14, AmsterdamMoscow 111250, Russian Federation*
[b]*National Research University "Bauman Moscow State Technical University", 2nd Baumanskaya 5, Moscow, 105005, Russian Federation*
[c]*JSC "Electrogorsk Research and Development Center on NPP Safety", Saint Constantine 6, Electrogorsk, Moscow Region, 142530, Russian Federation*

ARTICLE INFO

ABSTRACT

The results of the validation of the STEG code using the experiments on two-phase flow across horizontal tube bundles are presented. The experiments are carried out on two water–air SG models, consisting of a transparent vessels, inside of which there is a tube bundle, a perforated sheet and a bead separating the upstream section of the circulation circuit of the model from the downstream one. The void fractions and water velocities are measured in different locations of the models. The brief description of the STEG code based on the 3D two-fluid model is presented. A set of interfacial drag correlations, which was recently developed by the authors, are used in the validation calculations. The peculiarities of the spatial two-phase flows have been established, and a quantitative comparison with experimental data has been performed. Good agreement between the calculated and experimental data is obtained. About 90% of the experimental data points for both void fraction and water velocity are predicted by the STEG code with an accuracy of 10%.

1. Introduction

One of the main components of a nuclear power plant (NPP) with a pressurized water reactor is a steam generator (SG), the design of which largely determines the layout of the NPP, its cost and reliability. Horizontal SGs that generate saturated steam are employed in NPPs comprising Russian water-water energy reactors (WWERs) (Lukasevich et al., 2004; Papp and Vacek, 2017). The horizontal SG (Fig. 1) consists of a cylindricalshell in which U-shaped heat exchange tubes arranged in horizontal rows are connected to tubular vertical collectors for the supply (hot collector) and discharge (cold collector) of the heating coolant of the primary loop. Primary coolant from the reactor enters the SG through hot collector, travels through the horizontal heat exchange tubes, and exits through cold collector, transferring its heat to the secondary side water through the heat exchange surface wall. Due to the non-uniform heat release in the heat exchange tubes and the asymmetric arrangement of the internals, a complex three-dimensional flow takes place in the SG secondary circuit.

Subcooled feed water is supplied into the secondary side of the SG and is heated by mixing with saturated steam-water mixture available there. Saturated water flows down the corridors and then up through the tube bundles where steam is generated. Gravity separation is used to separate moisture from the steam in SG. The steam is removed from the SG through the steam outlet tubes in the upper part of the shell.

In the horizontal SG, the steam load at the outlet from the tube bundles is distributed non-uniformly along the horizontal cross-section of the SG, i.e., the steam load is the greatest in the hot collector (HC) zone (hot side) owing to the higher temperature of the primary heating coolant, and that in the cold collector (CC) zone (cold side) is the smallest. In order to equalize the steam load, submerged perforated sheets (SPSs) are installed in the horizontal SGs. An SPS is a device that has a high coefficient of hydraulic resistance, which makes it possible to equalize steam-water flows that are significantly non-uniform in space. Along the edges of the perforated sheet there is a vertical bead designed to ensure the natural circulation of the steam-water mixture. The SPS with the bead covers the tube bundle as a "cap", the gap between the outer surface of the bead and the vessel wall plays the role of a downcomer through which excess water from the horizontal plate of the sheet enters the lower part of the tube bundle.

The currently most common type of horizontal steam generator PGV1000 is designed for operation at nuclear power plants with WWER1000. It should be noted that over the course of about 20 years since the start of operation (1980), the PGV-1000 steam generators have been significantly modernized, retaining their name and basic concept (Lukasevich et al., 2004). The need for modernization was due to the exceptional complexity of the thermal–hydraulic processes occurring in the horizontal steam generator, which did not allow the most optimal solutions to be taken in advance at the design stage in some cases. Based on the results of experimental studies on full-scale steam generators and experimental models, a number of changes were made to the design of steam generators PGV-1000 (Lukasevich et al., 2004), as anexample, we indicate some of them: 1) installation of damper caps in the upper part of the SG vessel in the area of the hot collector to eliminate local steam ejection; 2) closure of the downcomer circulation channel in the heat exchange bundle to prevent the ejection of the steam-water mixture near the vessel wall; 3) change in the
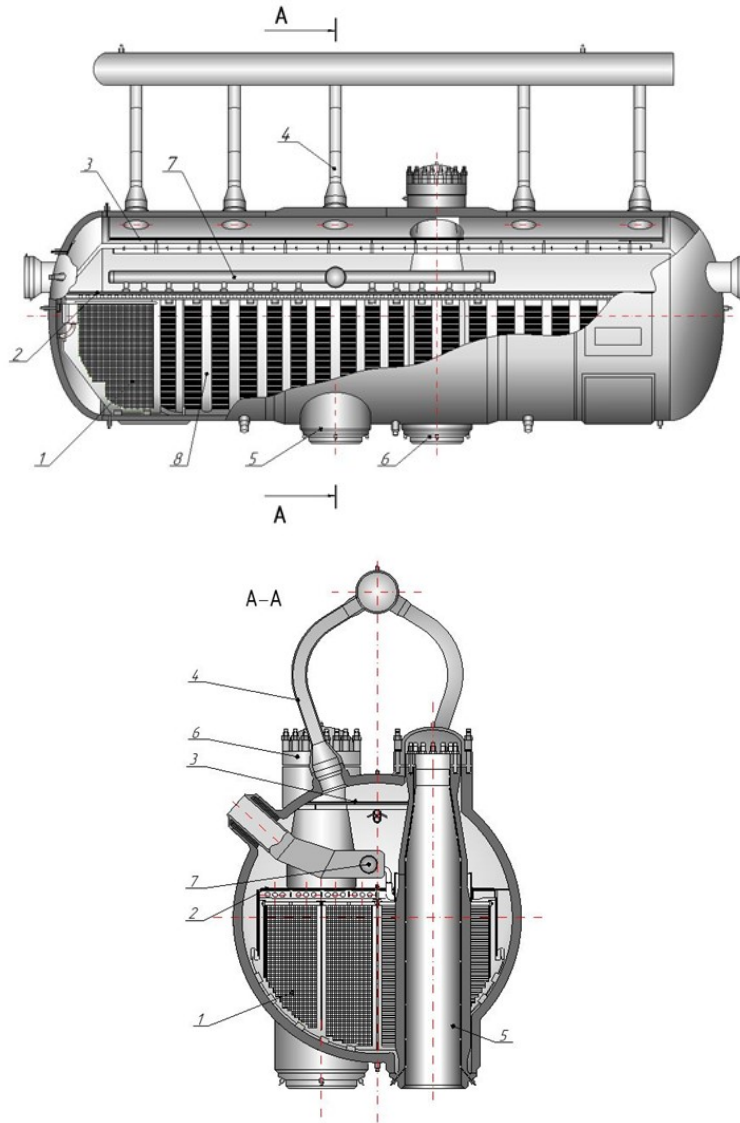
Figure 1: Sketch of WWER-1000 steam generator: (a) side view, (b) cross-section view. 1 – tube bundle, 2 - submerged perforated sheet, 3 –distribution perforated sheet, 4 – steam outlet tubes, 5 - hot collector, 6 - cold collector, 7 -feed water collector, 8 - tube support plates

value (increase) of the perforation degree of the submerged perforated sheet up to 8% in orderto improve the hydrodynamics of the water volume; 4) changes in the system of distribution of feed water and blowdown, in order to reduce the concentration of impurities in the area of hot collector; 5) optimization and reconstruction of the water level measurement system; 6) removal of a two-stage (chevron and vortex-vane) system for moisture separation and the use of gravity separation into the steam volume SG. From the above list of modifications, it follows that in order to optimize the SG internals, it is necessary to know the hydrodynamics of two-phase flows in the SG volume.

Thus, carrying out such experimental studies raised the question of the need to create special computer codes that simulate the hydrodynamics of two-phase flows in a horizontalsteam generator, which would allow performing optimization calculations for testing various design solutions. The main thermal–hydraulic problems that require research in the design of SG: 1) ensuring stable natural circulation of the steamwater mixture, which ensures reliable flow around the tubes and the absence of areas with poor heat transfer; 2) ensuring the design moisture of the generated steam through the use of separation devices (its provision is associated with the distribution of the heat release inside the steam generator, circulation of the steam-water mixture, equalization of the steam load, etc.); 3) vibration characteristics of the tube bundle; 4) distribution of dissolved impurities in the water volume and increasing the efficiency of blowing. Thus, the calculation codes must reliably predict the distribution of

the following main characteristics in the three-dimensional volume of the steam generator: void fraction, steam and water velocities, pressure drops on tube bundles, on SPS, etc., steam moisture, concentrations of dissolved impurities. The presence of such codes is especially important for the development of new high-power horizontal SGs (PGV-1200/1500).

Modeling of thermal hydraulics of horizontal SG was the subject of numerous works such as Melikhov et al. (1995a; b; c); Stosic and Stevanovic (2002); Stevanovic et al. (2002a;b); Maslovaric et al. (2004); Kroshilin et al. (2008); Zarifi et al. (2009); Hovi and Ilvonen (2010); Safavi et al. (2013); Ghazanfari et al. (2014); Rabiee et al. (2016; 2017), Le et al.(2021a). The detailed review of these works was presented by Le et al. (2020a). It can be concluded that the most suitable approach for the simulation of the hydrodynamic processes in a horizontal SG is the use of the 3D two-fluid model of the steam–water mixture with the consideration that the tube bundle is a porous medium. The key to the accurate description of the hydrodynamics of the horizontal SG is the interfacial drag force model and the pressure drop model of the steam–water mixture flow through the internal structures of the SG (tube bundle, submerged perforated sheet, etc.). Owing to the complexity of the developing 3D flows in horizontal SGs, the use of relevant experimental data is required to validate the selected closure correlations. To date, most of the researchers used only experimental data obtained on a full-scale WWER-1000 SG (Ageev et al., 1987) for a comparison with their calculated results. It should be mentioned that these experimental data are rather valuable and include readings from seventeen void fraction sensors installed in various tube-free SG zones (corridors, space between tube bundles and submerged perforated sheet, etc.). The void fraction was determined by measuring the hydrostatic pressure drop and the result of the measurement was an averaged void fraction over a sampling distance. But the shortcoming of this measurement was rather large the sampling distance (700–1000 mm), that makes it difficult to compare with the calculated data, since the typical dimensions of the computational cells are much smaller (50–100 mm) and it is necessaryto compare not the local value of the void fraction, but the value of the void fraction averaged over several cells with the experimental value. Such a procedure introduces some error and uncertainty, the local distributions of the parameters in the experiment and calculation may differ, but the values averaged over a sufficiently large distance may coincide. It is possible that the averaging of the void fraction at such a large distance was the reason that practically all the codes predicted the data well. Obviously, it is desirableto use additional experimental data to validate the thermal–hydraulic models of the horizontal SG.

Recently, Le et al. (2020a; b) validated the STEG code on experimental data obtained at the PGV test facility. The PGV test facility is a two-dimensional slice of the upper part of the horizontal WWER-1000 SG. The main components of the test facility are as follows: steam supply collector, tube bundle, submerged perforated sheet (SPS) and distribution perforated sheet. The five measurements of the void fraction below and above the SPS as well as behind the bead and the four pressure drops through the SPS are used. The operating pressure is 7 MPa and mass flow rate of the steam is 4–8 t/h. A total of 46 tests were performed with two different SPSs and spatially uniform and nonuniform steam supplies from the collector. All experiments were analyzed using the STEG code. A quantitative comparison with experimental data (SPS pressure drops and void fractions) was performed. The results generally indicated the relatively good predictive ability of the STEG code.

Le et al. (2021b) proposed a set of interfacial drag correlations for describing two-phase flows under thermal–hydraulic conditions of a horizontal SG. This set of correlations takes into account the peculiarities of the two-phase flow in different regions of the SG. These correlations were implemented in the STEG code, which was validated on the experimental data of the void fraction obtained at the PGV test facility (230 experimental points), the PGV-1500 model (60 experimental points) and the full-scale WWER-1000 SG (17 points). The main features of the PGV test facility and the full-scale WWER-1000 SG are mentioned above. The PGV-1500 model is a fragmentof a WWER-1500SG placed in a high pressure cylindrical vessel. The pressure in the test section of the model is 3.3 MPa. The test section includes heated and non-heated tube bundles, an SPS with a bead, and a distributed perforated sheet. The measurement system comprises twelve void fraction sensors in corridors, three void fraction sensors below the SPS, two differential pressure sensors on the SPS, and one differential pressure sensor on the heated tube bundle. In total, nine series of tests were performed using the PGV1500 hydrodynamic model. Good agreement between the calculated and experimental data was obtained. Thus, experimental data obtained at the PGV test facility, PGV-1500 model and full-scale WWER-1000 SG were used to validate the STEG code.

In the present study, previously unconsidered experimental data of Kolbasnikov (2000) are analyzed with the STEG code. A description of the SG experimental models, a brief overview of the STEG code, and calculation results are presented.

2. Brief description of SG experimental models and comparison with other test facilities

Experiments on two-phase air–water flow under typical conditions of a horizontal SG are presented by Kolbasnikov et al. (1991; 1992) and in more detail by Kolbasnikov (2000). Two SG experimental models were developed. The main components of Model 1 are a staggered tube bundle, a submerged perforated sheet and a downcomer, which are placed in a transparent vessel with dimensions of 364*500*3600 mm, Fig. 2. The tube bundle consists of 57 rows of 10 tubes, with tube length of 500 mm. Tubes with an outer diameter of 16 mm are arranged in staggered layout with transverse

spacing S1 = 19 mm and longitudinal spacing S2 = 23 mm, respectively, as in the WWER-1000 SG. The SPS is located 250 mm above the tube bundle. The downcomer is formed by the SPS bead and the vessel wall. In Model 1, the height of the bead is 1300 mm, it reaches the bottom tube of the tube bundle. In Model 2, the bead is shorter than in model 1, its height is 750 mm as in the WWER1000 SG. This is the only difference between SG Models 1 and 2. Two SPSs with perforation degrees of 4.5% and 7.5% are used in Model 1, and three SPSs with perforation degrees of 4.5%, 7.5% and 12% are used in Model 2 (perforation degree is the ratio of the area of the holes to the area of the sheet). Also tests without SPS are performed. The distance between the tube bundle and the left wall of the vessel is 82 mm, and the distance between the tube bundle and the SPS bead is 22 mm. The tube bundle is installed 500 mm above the bottom of the vessel.

Air is supplied in three sections along the height of the tube bundle, through all 10 perforated tubes located in each section, simulating the process of steam generation. These sections are located 30 mm, 600 mm and 870 mm above the lower boundary of the tube bundle, respectively. The flow rate of air supplied to each section may vary depending on the research program. The range of the superficial velocity of air is 0.07 2.0 m/s (air superficial velocity is defined as the ratio of the air volumetric flow rate to the cross-sectional area above the SPS). The direction of the water flow and its velocity are measured by turbine flow meters installed above the bundle, in tube-free and downcomer channels, no velocity measurement is realized inside the tube bundle. The turbine flowmeters is installed in casings, thereby eliminating the influence of lateral components of the flow velocity. Thus, the sensors can only measure the vertical component of the velocity, i.e. the amplitude and direction (up or down). A gamma densitometer is used to measure the local void fraction at various points in both along the width and height of the vessel. The relative measurement error of both velocity and void fraction is 10% according to Kolbasnikov (2000). The collapsed levels in the whole model (H1 for Model 1 and H1′for Model 2), below the SPS (H2) and above the SPS (H3) are determined by the hydrostatic method.

Each test is performed at a given air superficial velocity and water collapsed level. Test parameters for Model 1 and Model 2 are summarized in Tables 1 and 2, respectively. In addition to the air superficial velocity, the mass flow rate of the supplied air is also given.

Let us consider this SG model in a comparison with other test facilities simulating the thermal hydraulics of a horizontal steam generator, which were mentioned in the Introduction. The Table 3 summarizes the main parameters of the experimental installations PGV (Le et al., 2020a; b), PGV-1500 model (Le et al., 2021b) and SG model (Kolbasnikov, 2000), which is considered in this paper, and also provides information about the experiments conducted on a full-scale steam generator WWER-1000 SG (Ageev et al., 1987) and provides information on the main characteristics

Table 1
Test parameters for Model 1.

Test	Bottom air supply W_{01}'', m/s (G_{01}'', kg/s)	Middle air supply W_{02}'', m/s (G_{02}'', kg/s)	Top air supply W_{03}'', m/s (G_{03}'', kg/s)	H_1 m	H_2 m	H_3 m
Without SPS						
1.1	0 (0)	0 (0)	0.072 (0.014)	1.66	0.41	0.47
1.2	0 (0)	0 (0)	0.226 (0.044)	1.64	0.44	0.43
1.3	0.110 (0.021)	0.205 (0.040)	0.298 (0.058)	1.39	0.37	0.47
1.4	0.210 (0.041)	0.325 (0.063)	0.435 (0.085)	1.28	0.35	0.47
1.5	0.360 (0.070)	0.541 (0.105)	0.724 (0.141)	1.15	0.32	0.47
1.6	0.380 (0.074)	0.667 (0.130)	0.974 (0.189)	1.00	0.28	0.47
SPS with perforation degree 4.5%						
1.7	0 (0)	0 (0)	0.120 (0.023)	1.66	0.40	0.47
1.8	0 (0)	0 (0)	0.190 (0.037)	1.64	0.39	0.47
1.9	0 (0)	0 (0)	0.260 (0.051)	1.61	0.35	0.47
1.10	0.128 (0.025)	0.169 (0.033)	0.297 (0.058)	1.54	0.32	0.47
1.11	0.190 (0.037)	0.290 (0.056)	0.378 (0.073)	1.46	0.31	0.48
1.12	0.380 (0.074)	0.576 (0.112)	0.766 (0.149)	1.46	0.28	0.47
1.13	0.360 (0.070)	0.645 (0.125)	0.950 (0.185)	1.47	0.27	0.47
SPS with perforation degree 7.5%						
1.14	0 (0)	0 (0)	0.245 (0.048)	1.31	0.41	0.40
1.15	0.120 (0.023)	0.240 (0.047)	0.320 (0.062)	1.29	0.34	0.48
1.16	0.185 (0.036)	0.260 (0.051)	0.420 (0.082)	1.26	0.28	0.47
1.17	0.380 (0.074)	0.550 (0.107)	0.740 (0.144)	1.15	0.27	0.48
1.18	0.467 (0.091)	0.820 (0.159)	1.190 (0.231)	1.21	0.26	0.47

of the WWER-1500 SG horizontal steam generator project according to (Lukasevich et al., 2004). As follows from the Table 3, the SG model has the following specific features: 1) the steamwater mixture is modeled by the water–air mixture, 2) low pressure (slightly above atmospheric), 3) a wide range of average superficial air velocity at the interface surface 0.07–2.0 m/s, 4) staggered arrangement of tube bundle, 5) tube pitches corresponds to ones of the WWER-1000 SG, 6) three SPS with different perforation degree, 7) local void fractions were measured by gamma densitometer, 8) large number of tests (34). Thus, it can be concluded that the SG model reproduces the flow of a two-phase mixture under geometric conditions (in 2D geometry) of a full-scale SG,
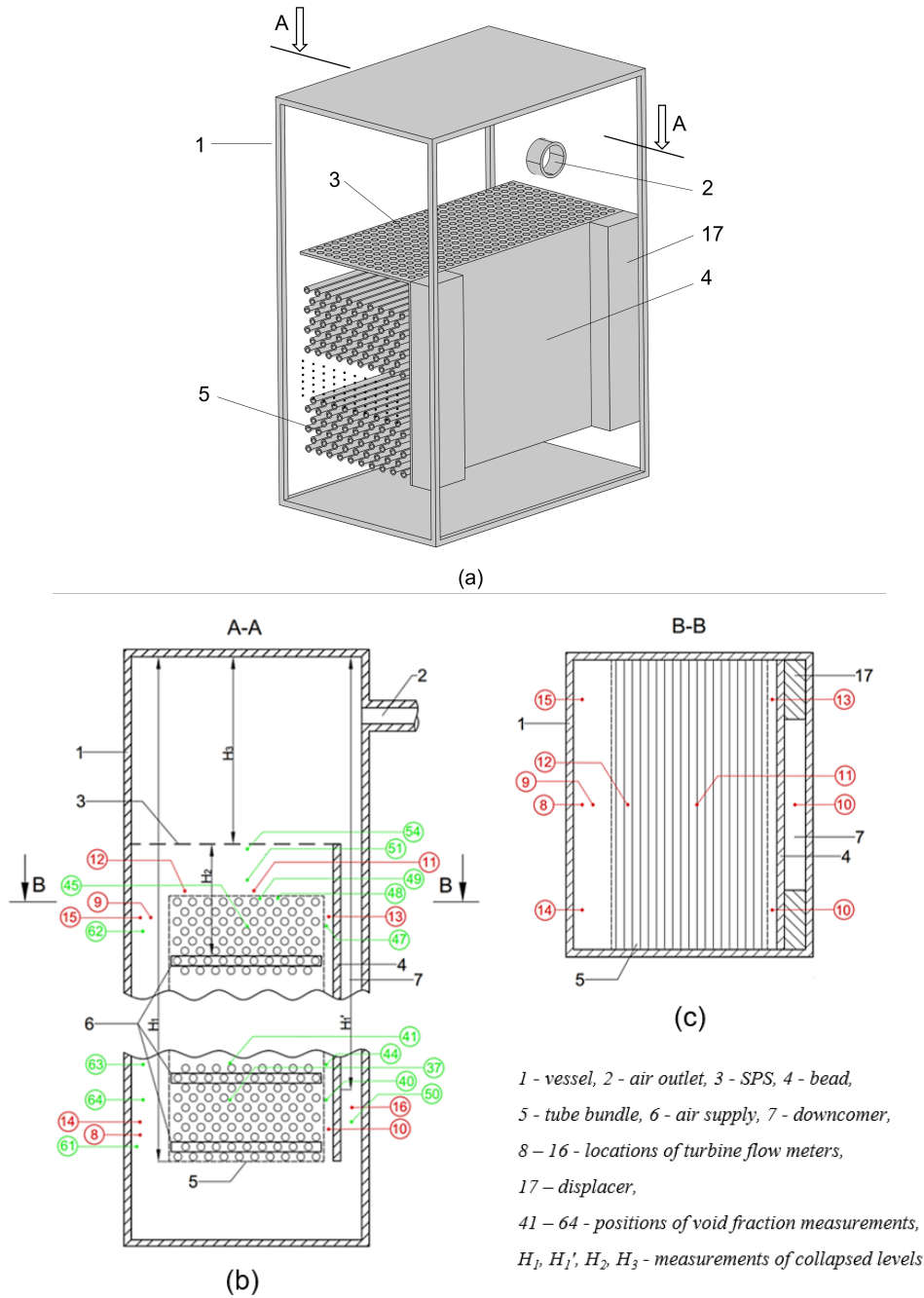
Figure 2: Schematic of Model 1: (a) general view, (b) cross-section view, (c) top cross-section view. 1 - vessel, 2 - air outlet, 3 - SPS, 4 - bead, 5 - tube bundle, 6 - air supply, 7 - downcomer, 8 − 16 - locations of turbine flow meters, 17 - displacer, 41 − 64 - positions of void fraction measurements

i.e. the experimental model has a tube bundle, an SPS with a bead, downcomer corridors whose geometric parameters correspond to WWER-1000 SG, the gas phase is supplied in a tube bundle. The flow rates of the supplied air provide a range of gas phase flow rates realized in WWER-1000 SG. However, in experiments, a water –air mixture at atmospheric pressure is used as a two-phase mixture, which differs significantly from natural conditions (steam-water mixture at a pressure of 6.27 MPa). Because of this, the ratio of the densities of the gas and water phase in the experiment is about 40 times different from the WWER-1000 SG ratio. Another significant difference between the SG model and the full-scale SG is the absence of heat release in the tube bundle and steam generation. The process of steam generation is simulated by means of air supply in the tube bundle. Nevertheless, despite the existing differences, it should be considered that the experimental data obtained on the SG model are quite valuable and expand and complement the

experimental data bank on horizontal SG thermal–hydraulic processes.

Table 2
Test parameters for Model 1.

Test	Bottom air supply W_{01}'',m/s $(G_{01}''$,kg/s)	Middle air supply W_{02}'',m/s $(G_{02}''$,kg/s)	Top air supply W_{03}'',m/s $(G_{03}''$,kg/s)	H_1 m	H_2 m	H_3 m
Without SPS						
2.1	0 (0)	0 (0)	0.220 (0.043)	1.34	0.32	0.47
2.2	0.118 (0.023)	0.261 (0.051)	0.353 (0.069)	1.34	0.33	0.48
2.3	0.310 (0.060)	0.465 (0.090)	0.621 (0.121)	1.28	0.32	0.48
2.4	0.427 (0.083)	0.631 (0.0123)	0.830 (0.0161)	1.27	0.31	0.48
2.5	0.550 (0.107)	0.850 (0.165)	1.140 (0.222)	1.15	0.32	0.47
SPS with perforation degree 4.5%						
2.6	0.312 (0.061)	0.470 (0.091)	0.636 (0.124)	1.30	0.23	0.47
2.7	0.428 (0.083)	0.711 (0.138)	0.994 (0.193)	1.32	0.23	0.47
SPS with perforation degree 7.5%						
2.8	0 (0)	0 (0)	0.180 (0.035)	1.35	0.33	0.47
2.9	0.196 (0.038)	0.304 (0.059)	0.427 (0.083)	1.35	0.33	0.47
2.10	0.282 (0.055)	0.414 (0.080)	0.553 (0.108)	1.31	0.26	0.47
2.11	0.376 (0.073)	0.567 (0.110)	0.745 (0.145)	1.30	0.26	0.47
2.12	0.469 (0.091)	0.711 (0.138)	0.930 (0.181)	1.31	0.26	0.47
SPS with perforation degree 12%						
2.13	0.266 (0.052)	0.382 (0.074)	0.493 (0.096)	1.37	0.27	0.48
2.14	0.305 (0.059)	0.479 (0.093)	0.648 (0.126)	1.28	0.26	0.46
2.15	0.433 (0.084)	0.631 (0.123)	0.838 (0.163)	1.28	0.26	0.46
2.16	0.524 (0.102)	0.801 (0.156)	1.050 (0.204)	1.26	0.24	0.47

3. Brief description of STEG code

The simulation of a two-phase gas–liquid flow is based on a threedimensional (3D) two-fluid model. The mass, momentum and energy balances are formulated for each phase, which requires closure relationships for interfacial interactions and interactions with surrounding structures; the SG tubes are considered as a porous medium. Flow governing equations are written in the non-viscous form, while laminar or turbulent viscosity effects are indirectly considered in the form of friction coefficients for the tube-bundle or SPS flow resistance and twophase interfacial drag force.

The air–water flow considered in this study is isothermal, so there is no interfacial heat exchange. For brevity, the energy equations and terms related to phase change as well as correlations for heat transfer are not provided here. Note that

the momentum equations are written in a non-conservative form as in (TRAC–PF1/MOD2., 1990; RELAP5/ Mod3.3, 2001), which is suitable for application of semi-implicit numerical method (Liles and Reed, 1978).

3.1. Mass conservation
Liquid.

$$\frac{\partial \alpha_l \rho_l}{\partial t} + div\left(\alpha_l \rho_l \vec{V}_l\right) = M_{s,l} \tag{1}$$

Gas.

$$\frac{\partial \alpha_g \rho_g}{\partial t} + div\left(\alpha_g \rho_g \vec{V}_g\right) = M_{s,g} \tag{2}$$

3.2. Momentum conservation
Liquid.

$$\frac{\partial \vec{V}_l}{\partial t} + \vec{V}_l \cdot \nabla \vec{V}_l = -\frac{1}{\rho_l}\nabla p + \frac{C_i d}{\alpha_l \rho_l}|\vec{V}_g - \vec{V}_l|(\vec{V}_g - \vec{V}_l) \\ - \frac{\vec{F}_{TBl}}{\alpha_l \rho_l} + \vec{g} + \frac{M_{s,l}(\vec{V}_{s,l} - \vec{V}_l)}{\alpha_l \rho_l} \tag{3}$$

Gas.

$$\frac{\partial \vec{V}_g}{\partial t} + \vec{V}_g \cdot \nabla \vec{V}_g = -\frac{1}{\rho_g}\nabla p + \frac{C_i d}{\alpha_g \rho_g}|\vec{V}_g - \vec{V}_l|(\vec{V}_g - \vec{V}_l) \\ - \frac{\vec{F}_{TBg}}{\alpha_g \rho_g} + \vec{g} + \frac{M_{s,g}(\vec{V}_{s,g} - \vec{V}_g)}{\alpha_g \rho_g} \tag{4}$$

3.3. Volume fraction balance

$$\alpha_l + \alpha_g + \alpha_{tubes} = 1 \tag{5}$$

The index l is liquid and g – gas, α_l, α_g – volume fractions of liquid and gas, respectively, ρ – density, $\vec{V}$ – velocity, p – pressure, $M_{s,l}$, $M_{s,g}$ – mass sources of liquid and gas, respectively, C_{id} – interfacial shear coefficient, $\vec{F}_{TBl}$, $\vec{F}_{TBg}$ – drag forces of tube bundle and liquid and gas, respectively, $\vec{F}_{SPSg}$ – drag force of SPS and gas, $V_{s,l}$, $V_{s,g}$ – velocities of liquid and gas, supplied from sources, respectively, $\vec{g}$ – gravity.; α_{tubes} – volume fraction of the tube bundle.

3.4. Interfacial drag
Le et al. (2021b) proposed a set of interfacial drag correlations for describing interfacial friction in different SG zones. Let us briefly outline its features.

3.4.1. Characteristic regions of the steam-water mixture flow in a horizontal SG
Measurements of the void fractions in full-scale horizontal SGs and experimental models of SGs (Trunov et al., 2001) allow us to select four characteristic regions in which the two-phase flow has its own peculiarities.

Region I: Tube bundles. In tube bundles, the void fraction varies from 0 (in the lower part) to 0.8 (in the upper part). Bubble and churnturbulent flows are observed.

Table 3
Main technical parameters of the test facilities and SGs.

Parameter	PGV test facility	PGV-1500 model	SG model	WWER-1000 SG	WWER-1500 SG
Operation					
Working fluid	steam-water	steam-water	air-water	steam-water	steam-water
System pressure, MPa	7	3.3	0.1	6.27	7.34
System temperature, °C	285.8	239.2	20	278.5	288.9
Thermal power, MW	0	2.5	0	750	1062.5
Steam generation by heating tubes or steam/air supply from collectors	steam supply	heating tubes + steam supply	air supply	heating tubes	heating tubes
Steam/air mass flow rater, t/h	4-8	6-10	0.05-14	1470	2067
Feed water supply	no	yes	no	yes	yes
Average superficial steam/air velocity m/s	0.15-0.29	0.24-0.56	0.07-2.0	0.31	0.28
Geometry					
Vessel	2D cross-section slice of the horizontal SG			cylinder	cylinder
Vessel dimensions, m	2.37/1.62/0.1	2.25/2.25/0.25	0.364/3.6/0.5	13.4/4.0	15.6/4.7
Number of tube bundles	1	2	1	4	4
Tube bundle arrangement	in-line	in-line	staggered	staggered	in-line
Tube pitches, mm	22/24	22/24	19/23	19/23	22/24
Tube diameter, mm	16	16	16	16	16
Number of tubes	255	1944	570	11000	15120
SPS perforation degree, %	5.7,4.1,8.3	10.62	4.5,7.5,12	3.7,6.1	not defined yet
Measurements					
Void fraction	5	15	15	16	-
Water velocity	0	4	9	5	-
Pressure difference	4	3	0	0	-
Collapsed level	2	3	3	1	-
Number of tests	44	9	34	1	-

Region II: Tube-free zones in the SG lower part (corridors between tube bundles, side gaps, end gaps). The void fraction here does not exceed 0.5. Typical widths of corridors and gaps are 130–250 mm, so these objects can be classified as large diameter channels, in which the influence of the walls on the characteristics of the two-phase flow is insignificant. Indeed, according to Schlegel and Hibiki (2015), the transition between small and large diameter systems occurs in the range of diameters $D_h = (18 \div 52) \cdot Lo$, where $Lo = \sqrt{\sigma/(g\Delta\rho)}$ is the capillary length. At a typical SG pressure of 7 MPa this transition range is $27 \div 78$ mm. Therefore, according to results of Ohnuki and Akimoto (2000), Schlegel et al. (2009), Shen et al. (2014), in whichthe two-phase flow in large diameter channels were analyzed, in this region the typical flow regimes are bubbly and cap-bubbly ones.

Region III: Zone between the outlet from the tube bundles and the SPS. In this region, the characteristic values of the void fraction are 0.5–1.0, which corresponds to churn-turbulent and mist flows.

Region IV: SG upper part (bubbling layer above the SPS and the steam volume). At the initial section of the bubbling layer, steam jets flowing out of the SPS holes break up into bubbles of various sizes. Then these bubbles flow upward in the stabilized section, while the void fraction is 0.3–0.5, which corresponds to cap-bubbly flow. Further on the evaporation surface, the steam leaves the bubbling layer, capturing water droplets, and enters the steam region.

Table 4 summarizes the flow regimes observed in a horizontal SG.

Table 4
Flow regimes in different regions of SG.

Region	Regime			
	Bubbly	Capbub-bly	Churntu-rbulent	Mist
I. Tube bundle	+	−	+	+
II. Tube-free zones in SG lower part (corridors, etc.)	+	+	−	−
III. Zone between the outlet from the tube bundle and the SPS	−	−	+	+
IV. SG upper part (above the SPS)	−	+	−	+

The interfacial drag force per unit volume $\vec{F}_{id}$ is given by:

$$\vec{F}_{id} = 0.75 \frac{C_D}{D_p} \rho_c \alpha_d \vec{V}_r |\vec{V}_r| \qquad (6)$$

Here C_D – drag coefficient, D_p – particle diameter, ρ_c – density of continuous phase, α_d – void fraction of dispersed phase, $\vec{V}_r = \vec{V}_d - \vec{V}_c$ – relative velocity, $\vec{V}_d$ – velocity of dispersed phase, $\vec{V}_c$ – velocity of continuous phase.

The following characteristic regions are distinguished in the horizontal steam generator.

3.4.2. Region I: Tube bundles.

Simovic et al. (2007) model is used. Depending on the value of the void fraction $\alpha = \alpha_g/(\alpha_l + \alpha_g)$, three flow regimes are distinguished:

Bubbly flow ($0 \le \alpha \le 0.3$). The ratio of C_D/D_p is given by the modified Ishii and Zuber (1979) correlation.

$$\frac{C_D}{D_P} = 0.267 \left(\frac{g\Delta\rho}{\sigma}\right)^{0.5} \left[\frac{1 + 17.67 f(\alpha)^{6/7}}{18.67 f(\alpha)}\right]^2 \quad (7)$$

where g – gravity, $\Delta\rho$ – density difference, σ – interfacial tension, $f(\alpha) = (1-\alpha)^{1.5}$.

Churn-turbulent flow ($\alpha > 0.3$ and $(\alpha V_g) < 15$ m/s). A correlation is used with the same functional form, as the CATHARE code (Rousseau and Houdayer, 1983).

$$\frac{C_D}{D_P} = 1.487 \left(\frac{g\Delta\rho}{\sigma}\right)^{0.5} (1-\alpha)^3 (1-0.75\alpha)^2 \quad (8)$$

Annular and/or mist flow ($\alpha > 0.3$ and $(\alpha V_g) > 15$ m/s). For annular and mist flow patterns, C_D is proportional to the square of the gas velocity (Rousseau and Houdayer, 1983).

$$\frac{C_D}{D_P} = 7.136 \cdot 10^{-5} \left(\frac{g\Delta\rho}{\sigma}\right)^{0.5} (1-\alpha)|\vec{V}_g|^2 \quad (9)$$

3.4.3. Regions II, III, IV.

Bubbly flow ($0 \le \alpha \le 0.2$). In the range of the low void fractions the shape of bubbles is assumed to be spherical and the drag coefficient should be given as function of Reynolds number (viscous regime).

$$C_{D1} = \frac{24}{Re_p}(1+0.15Re_p^{0.687}), \ D_P = 2Lo, \ Lo = \sqrt{\sigma/(\Delta\rho \cdot g)}$$
$$(10)$$

where $Re_P = D_P V_r \rho_l/\mu_l$ – Reynolds number, D_P – bubble diameter, μ_l – viscosity of liquid.

Bubbly-cap flow ($0.3 \le \alpha \le \alpha_{CT}$). The values of α_{CT} for the zones under and above the SPS are 0.5 and 0.7, respectively. The parameter α_{CT} was determined by comparing calculated and experimental data in (Le et al., 2021b). The flows of a two-phase steam-water mixture in the area below the SPS and above the SPS have different features, as shown in (Le et al., 2021b), so α_{CT} has different values. Bubbles are divided into two groups: 1) small slightly distorted bubbles (Group-1) and 2) large cap bubbles (Group-2). The interfacial drag force between the Group-1 bubbles, Group-2 bubbles and liquid per unit volume is determined as follows:

$$\vec{F}_{id} = 0.75\frac{C_{D1}}{D_{P1}}\rho_l\alpha_{g1}\vec{V}_{r1}|\vec{V}_{r1}| + 0.75\frac{C_{D2}}{D_{P2}}\rho_l\alpha_{g2}\vec{V}_{r2}|\vec{V}_{r2}| \quad (11)$$

where $\vec{V}_{r1} = \vec{V}_{g1} - \vec{V}_l$ – relative velocity of the Group-1 bubbles, $\vec{V}_{r2} = \vec{V}_{g2} - \vec{V}_l$ – relative velocity of the Group-2 bubbles.

For Group-1 bubbles, the distorted fluid particle regime occurs where the drag coefficient depends only on the particle radius and fluid properties and not on the velocity or the viscosity (Ishii and Zuber, 1979)

Group-1

$$\frac{C_{D1}}{D_{P1}} = \frac{2}{3}\left(\frac{g\Delta\rho}{\sigma}\right)^{0.5}\left(\frac{1 + 17.67(1-\alpha_{g1})^{1.3}}{18.67(1-\alpha_{g1})^{1.5}}\right)^2 \quad (12)$$

where α_{g1} - volume fraction of Group-1 bubbles.

The drag coefficient of Group-2 bubbles is determined with the correlation for churn-turbulent flow (Ishii and Zuber, 1979). A cap bubble diameter equal to 40Lo (TRAC, 1990).

Group-2

$$C_{D2} = \frac{8}{3}(1-\alpha)^2, \ D_{P2} = 40Lo \quad (13)$$

where α_{g2} - volume fraction of Group-2 bubbles.

The Group-1 and Group-2 void fractions are given by the model of Ozar et al. (2012).

$$\alpha_{g1} = \begin{cases} \alpha, & \alpha \le 0.25 \\ 0.51(1 - \frac{\alpha-0.25}{0.51-0.25}), & 0.25 < \alpha \le 0.51 \\ 0, & 0.51 < \alpha \end{cases} \quad (14)$$

$$\alpha_{g2} = \alpha - \alpha_{g1} \quad (15)$$

According to this model, α_{g1} is equal to total void fraction before the transition from bubbly to cap-bubbly flow regime. The transition point is denoted as $\alpha_{g1,\max}$. Beyond this point, α_{g1} starts decreasing due to coalescence of bubbles and approaches to an asymptotic value at a certain value of void fraction which is denoted as α_{crit}. Once this point is reached, α_{g1} does not change significantly and become a constant value. This asymptotic value of α_{g1} is defined as $\alpha_{g1,base}$. The parameter α_{crit} is defined as 0.51 based on the condition of maximum packing of cap bubbles (Shen et al., 2014). Two other parameters $\alpha_{g1,\max}$ and $\alpha_{g1,base}$ were estimated in (Le et al. 2021b) as $\alpha_{g1,\max} = 0.25$; $\alpha_{g1,base} = 0$ (below the SPS) and $\alpha_{g1,\max} = 0.15$; $\alpha_{g1,base} = 0.05$ (above the SPS).

Since only one velocity field is used to describe the gas flow, the expression for the interfacial force is written in terms of this velocity, which is some effective velocity of movement of two groups of bubbles.

$$\vec{F}_{id} = 0.75\frac{C_{D,\text{eff}}}{D_{P,\text{eff}}}\rho_l\alpha_g\vec{V}_{r,\text{eff}}|\vec{V}_{r,\text{eff}}| = C_{id,\text{eff}}\cdot\vec{V}_{r,\text{eff}}|\vec{V}_{r,\text{eff}}| \quad (16)$$

The index eff means effective, i.e. one effective parameter describes the average behavior of two groups of bubbles.

From Eqs. (11) and (16) we obtain

$$C_{id,\text{eff}} = 0.75\frac{C_{D1}}{D_{P1}}\rho_l\alpha_{g1}\frac{\vec{V}_{r1}}{\vec{V}_{r,\text{eff}}}\frac{|\vec{V}_{r1}|}{|\vec{V}_{r,\text{eff}}|} + $$
$$0.75\frac{C_{D2}}{D_{P2}}\rho_l\alpha_{g2}\frac{\vec{V}_{r2}}{\vec{V}_{r,\text{eff}}}\frac{|\vec{V}_{r2}|}{|\vec{V}_{r,\text{eff}}|} \quad (17)$$

It is necessary to determine relations between relative velocities $\vec{V}_{r1}$, $\vec{V}_{r2}$ and effective relative velocity $\vec{V}_{r,\text{eff}}$. Let us consider for simplicity the one-dimensional vertical upward motion of bubbles in a motionless liquid. The well-known expression is obtained from the momentum balances of liquid and vapor (Wallis, 1969).

$$\alpha_g(1 - \alpha_g)\Delta\rho g = F_{id,z} \tag{18}$$

Eq.(18) is applied to each group of bubbles.
Group-1

$$\alpha_{g1}(1 - \alpha_{g1})g\Delta\rho_{g1} = 0.75\frac{C_{D1}}{D_{P1}}\rho_l\alpha_{g1}V_{r1,z}^2 \tag{19}$$

Group-2

$$\alpha_{g2}(1 - \alpha_{g2})g\Delta\rho_{g2} = 0.75\frac{C_{D2}}{D_{P2}}\rho_l\alpha_{g2}V_{r2,z}^2 \tag{20}$$

where $\Delta\rho_{g1} = \frac{(\alpha_{g2}\rho_g + 1(1-\alpha)\rho_l)}{1-\alpha_{g1}}$, $\Delta\rho_{g2} = \frac{(\alpha_{g1}\rho_g + 1(1-\alpha)\rho_l)}{1-\alpha_{g2}}$.

The sum of the superficial velocities of the Group-1 and Group-2 bubbles must equal the superficial gas velocity.

$$\alpha_{g1}V_{g1,z} + \alpha_{g2}V_{g2,z} = \alpha V_{g,z} \tag{21}$$

From Eq.(21) it is easy to obtain an expression for the relative velocities.

$$\alpha_{g1}V_{r1,z} + \alpha_{g2}V_{r2,z} = \alpha V_{r,z,\text{eff}} \tag{22}$$

From Eqs. (19), (20), and (22), we obtain the required relations for Eq.(17).

Churn-turbulent flow (only below the SPS, $0.5 < \alpha < 0.7$).

For this regime, the drag coefficient and the average diameter of a churn-turbulent bubble is defined as:

$$C_D = \frac{8}{3}(1 - \alpha)^2, \ D_P = 20Lo \tag{23}$$

Mist flow ($\alpha_{CM} < \alpha < 1.0$).

As shown in (Le et al./ 2021b), the lower boundary of mist flow α_{CM} depends on the shape of the water droplets (distorted or spherical shapes). The average droplet diameter is determined by experimental correlation (Ageev et al., 1988) as follows:

$$D_d = 1.67Lo\left(\frac{j_{g,ev}^2\rho_g Lo}{\sigma}\right)^{0.42}\left(\frac{\rho_g}{\rho_l}\right)^{0.29} \tag{24}$$

where $j_{g,ev}$ – gas superficial velocity on the surface between gas and gas-liquid mixture.

If the diameter of droplets exceeds the critical value $D_{d,crit} = 69.3(\rho_g g\Delta\rho/\mu_g^2)^{-0.333}$ (Ishii and Zuber, 1979), then the droplets have a distorted shape, accordingly, the drag coefficient is defined as:

$$\frac{C_D}{D_d} = \frac{2}{3}\left(\frac{g\Delta\rho}{\sigma}\right)^{0.5}\left(\frac{1 + 17.67f(\alpha)^{6/7}}{18.67f(\alpha)}\right)^2, \ f(\alpha) = \alpha^3 \tag{25}$$

In this case, the value of α_{CM} is 0.8.

When the diameter of droplets is less than the critical value, then the droplets become to spherical particles and there is a viscous flow regime.

$$C_D = \frac{24}{Re_d}(1 + 0.1\cdot Re_d^{0.75}), \ Re_d = \frac{\rho_g D_d V_r}{\mu_m}, \ \mu_m = \frac{\mu_g}{(1 - \alpha_d)^{2.5}} \tag{26}$$

For this regime α_{CM} is 0.9. All relations of the interface drag force presented above are summarized in Table 5.

3.5. Tube bundle pressure drop

The total pressure drop of two-phase flow on the tube bundle in the direction of the e coordinate axis (e = x,y,z) is determined as follows:

$$\Delta P_{2\phi} = \xi_0\frac{G^2}{2\rho_l}\Psi\left[1 + x\left(\frac{\rho_l}{\rho_g} - 1\right)\right] \tag{27}$$

where ξ_0 – single-phase loss coefficient, G – mass flux, Ψ – non-homogeneous multiplier, x – quality. The non-homogeneous multiplier Ψ is calculated based on experimental data (Kolbasnikov et al., 1991, 1992).

The corresponding total drag force between the tube bundle and twophase flow is calculated as follows

$$\vec{F}_{2\phi} = (1 - \alpha_{tubes})\frac{\Delta P_{2\phi}}{\Delta e}\vec{e} \tag{28}$$

where Δe is the width of the computational cell in the e direction, $\vec{e}$ denotes unit vector.

The division of the total force $\vec{F}_{2\phi}$ into two forces defining a separate contribution of the each phase is done using the approach proposed in (RELAP5/Mod3.3, 2001). Its essence is as follows: first, preliminary values of the drag force on the tube bundle for the liquid phase and for the gas phase are calculated, obtained using correlations for a singlephase flow according to the thermophysical and hydrodynamic parameters of each phase. Then they are renormalized so as to sum up to give the total force of the two-phase flow on the tube bundle. As a result, the resulting forces have the following form

$$\vec{F}_{TBl} = \alpha_l\vec{F}_{2\phi}\left(\frac{z_\phi}{\alpha_g + \alpha_l z_\phi}\right) \tag{29}$$

$$\vec{F}_{TBg} = \alpha_g\vec{F}_{2\phi}\left(\frac{1}{\alpha_g + \alpha_l z_\phi}\right) \tag{30}$$

Here so-called z-factor z_phi is determined as

$$z_\phi = \frac{|\vec{F}_{TBl}|/\alpha_l}{|\vec{F}_{TBg}|/\alpha_g} \tag{31}$$

To estimate it, the relations for $|\vec{F}_{TBl}|$, $|\vec{F}_{TBg}|$ are used, for the singlephase case (RELAP5/Mod3.3, 2001).

3.6. SPS pressure drop

Ryabov et al. (1984) proposed to determine the pressure drop on the SPS as:

$$\Delta P_{\text{SPS}} = \Delta P_g \cdot \chi_{\text{SPS}} \tag{32}$$

which in the notation of our work can be represented as follows:

$$\Delta P_{\text{SPS}} = \xi \cdot \left[\frac{\rho_g (\alpha_g V_{gz})^2}{2} \right]_{\text{SPS}} \cdot \chi_{\text{SPS}} \tag{33}$$

where ξ – SPS single-phase loss coefficient (Idelchik, 1992), ρ_g – gas density, V_{gz} – vertical gas velocity in the SPS holes (in z-direction), respectively, $\alpha_g V_{gz}$ – vertical superficial gas velocity in the SPS holes, χ_{SPS} – multiplier.

This expression means that the basis of the calculation of the pressure drop on the SPS is the pressure loss caused by the steam flow and further refinement is made by the multiplier χ_{SPS}, which takes into account the presence of water in the flow through the SPS. This recommendation is based on the fact that in the experimental studies of the two-phase hydrodynamics of the SPS the steam flow rate always is given through which the experimental data on pressure drops are expressed.

The multiplier χ_{SPS} depends on the geometry of the hole, pressure, and void fraction of the two-phase flow below the SPS. For SG conditions in the works of Melikhov et al. (2015a, b, 2018) and Blinkov et al. (2015, 2016), respectively, based on the experimental data processing, a correlation was obtained for χ_{SPS} depending on the void fraction below the SPS:

$$\chi_{\text{SPS}} = 1.64 - 1.18 \cdot \alpha_{g,\text{SPS}} \tag{34}$$

where $\alpha_{g,SPS}$ is the void fraction under the SPS.

The force from the SPS acts on the gas only in the vertical direction and is calculated as follows

$$F_{\text{SPS}g,x} = F_{\text{SPS}g,y} = 0, \ F_{\text{SPS}g,z} = \frac{\Delta P_{\text{SPS}}}{\Delta z} \ for \ z = h_{\text{SPS}} \tag{35}$$

where h_{SPS} - height of SPS, Δz - size of the computational cell near SPS.

4. Validation of STEG code against experiments

4.1. Numerical method, nodalization scheme and calculation procedure

Set of equations (1)-(5) is solved by the finite-difference semi-implicit method (Liles and Reed, 1978, TRAC–PF1/MOD2, 1990). The STEG code uses a staggered-grid scheme in which the velocities are defined at the grid-cell interfaces and the pressure, volume fractions and densities are defined at the grid-cell centers. The scalar field equations (mass) apply to a grid cell, whereas the velocity component momentum equations apply to an interface between grid cells

in the three velocitycomponent directions. The convective terms are approximated with upwind finite differences (first order of accuracy). Semi-implicit time integration is applied, i.e. the convective terms in the mass equations, the pressure gradient terms in the momentum equations, and all source terms contain terms evaluated at the new time level. Such semi-implicit approximation makes it possible to remove significant restrictions on the value of the integration time step. The transient calculation procedure is performed within the following steps:

1. Calculation of preliminary liquid and gas velocity components from projections of Eqs. (3) and (4) using pressure gradient terms at the old time level.

2. Solving of pressure equation, obtained by combining the mass and momentum conservation equations.

3. Calculation of velocity components and volume fractions of liquid and gas from Eqs. (1) - (4) using the current pressure from Step 2.

4. Steps 2 and 3 are repeated until the solution converges. 5. Time is increased and for the new time step of integration new values are assigned as initial ones. Also, the physical properties are updated. The calculation procedure is continued with step 1.

To simulate the experiments, a nodalization scheme is developed, as shown in Fig. 3. The dimensions of the simulation domain are 364 mm and 3600 mm in horizontal and vertical direction, respectively. A hexahedral structured mesh is employed with a staggered arrangement of velocity components, which are stored at the cell faces, and scalar variables, which are stored at the cell nodes. The nodalization scheme is the same for both Model 1 and Model 2. The air supply is modeled by mass gas sources $M_{s,g}$ (see Eq. (1)) located in three sections along the height of the tube bundle (Fig. 2).

The grid dependency tests have been performed with 8 × 62, 16 × 124, and 32 × 248 (in the horizontal and vertical directions, respectively; 1 cell is utilized for the width of the model). Corresponding cell sizes – 46 × 58 mm, 23 × 29 mm and 11.5 × 14.5 mm, respectively. The averaged void fraction in the tube bundle $\alpha_{aver} = 0.2 \cdot (\varphi_{37} + \varphi_{41} + \varphi_{45} + \varphi_{48} + \varphi_{49})$ and averaged velocity in the free channels $w_{aver} = 0.25 \cdot (w_8 + w_9 + w_{10} + w_{13})$ were compared for three experiments at Model 1. The results thus obtained are presented in Fig. 4. The computer costs (laptop Lenovo Legion Y9000P) for the calculation of 300 s of the process, required to reach the steady state, are 8 h (grid 16 × 124) and 60 h (grid 32 × 248) (almost 8 times longer). So, in terms of trade-off between computation time and model accuracy the grid comprising 16 × 124 cells are selected for further calculations.

At the initial moment of time, water is placed in the lower part of the computational domain, whereas air is introduced into the upper part. Thereafter, the air flow is switched on at the required rate and calculations are initiated. The amount of water is regulated using a mass source so that the calculated collapsed level in the whole model (H1 for Model 1 and H1 for Model 2) is equal to the experimental value. Fig. 5 shows the typical behavior of the calculated void fractions

Table 5
Interfacial drag correlations of the STEG-M code. Region

Region	Void fraction					
	$0<\alpha<0.2$	$0.2\leq\alpha<0.3$	$0.3\leq\alpha<0.5$	$0.5\leq\alpha<0.7$	$0.7\leq\alpha<\alpha_{cm}$	$\alpha_{cm}\leq\alpha<1$
I. Tube bundle	Bubbly flow, Eq.(7)	Churn-turbulent flow ($\alpha > 0.3$ and $(\alpha V_g) < 15$ m/s), Eq.(8); Annular/mist flow ($\alpha>0.3$ and $(\alpha V_g) > 15$ m/s), Eq.(9)				
II. Tube-free zones in SG lower part (corridors, etc.)	Bubbly flow Eq.(10) $D_{p1} = 2\cdot Lo$	Linear interpolation	Churn-turbulent flow Eq.(23)	Bubbly-cap flow Eqs.(11),(12),(13), (14),(15),(17)	Liner interpolation	Mist flow, Eq.(24) If $D_d < D_{d,crit}$, then Eq.(26)
III. Zone between the outlet from the tube bundle and the SPS					Liner interpolation	Mist flow, Eq.(24) If $D_d \geq D_{d,crit}$, then Eq.(25)
IV. SG upper part (above the SPS) Operation	Bubbly-cap flow Eqs.(12),(13),(14),(15),(16),(17)					

as a function of time. The calculation continues until a steady state is reached (t = 250 s). The steady state is maintained for 50 s (between 250 s and 300 s). The solution is oscillatory; hence, all calculated parameters are averaged over time. The time step is 0.001 s.

All Figures in the following sections show not instantaneous, but averaged parameters over a time interval of 250–300 s.

4.2. Comparison of calculation results and experimental results

Let us consider the main features of the flow of a two-phase mixture. Fig. 6 shows the distribution of the void fraction and superficial air and water velocities for two experiments Test 1.6 (without SPS) and Test 1.13 (SPS perforation degree 4.5 %) with similar parameters for the supply air flow rate and the water level in the vessel. On the whole, the pattern of the air–water mixture flow in the experiments without SPS and with SPS is approximately the same. In the tube bundle, where air is supplied, an upward flow of the air–water mixture occurs, after leaving the tube bundle, the air continues to move upward, and the water slows down due to gravity. As a result, an interface is formed that separates the two-phase two-phase mixture from the air in the upper part of the vessel. The water carried up through the tube bundle then descends into the lower part of the vessel along the side boundaries. The presence of SPS (Test 1.13) leads to an increase in the void fraction under the SPS due to the large hydraulic resistance of the SPS.

The influence of the bead length on the flow pattern is small. Fig. 7 shows the distributions of void fraction and superficial air and water velocities for experiments with SPS perforation degree of 7.5 % and similar air flow rates and water levels in the vessel for Model 1 and Model 2, respectively. In the case of a shorter bead (Test 2.11), in the lower right part of the vessel, the air partially escapes from the tube bundle to the right towards the vessel boundary and a region with a slightly increased void fraction is formed compared to Test 1.17 with a long bead.

A decrease in the flow rate of the supplied air leads to a decrease in the flow of water into the upper part of the vessel and, thereby, an in- crease in the volume fraction of water in the lower part of the vessel, Fig. 8.

A comparison of numerical and experimental data on void fractions and water velocities for Model 1 and Model 2 is presented in Fig. 9a and b, respectively. It can be seen that the error band of ±15 % covers a significant number of points. Recall that the local void fraction was measured by gamma densitometer and vertical component of the water velocity was measured by turbine flowmeters in the experiments. The STEG code for all tests has predicted the direction of water movement (up or down) correctly, so the following are only a comparison of calculated and experimental amplitudes.

Figs. 10-12 present some typical graphs that illustrate the comparison of calculated and experimental data on void fractions and water velocities. The distributions of the void fraction along the height in a large free channel (sensors 61, 62, 63, 64), a tube bundle (sensors 37, 41, 45) and a small free channel (sensors 40, 44, 47), as well as distributions of water velocity in large free channel (sensors 14 and 15) and small free channel (sensors 10 and 13). Good agreement of calculated and exper- imental data is observed.

To characterize the differences between the experimental and calculated values, we use the mean absolute deviation (MAD) and the maximum absolute error (MAXE), which are defined as

$$\text{MAD} = \frac{1}{N}\sum_{i=1}^{N}\frac{|f_{\text{exp},i} - f_{\text{calc},i}|}{|f_{\text{exp},i}|}\cdot 100\%,\ i = 1...N \quad (36)$$

$$\text{MAXE} = \max\left(\frac{|f_{\text{exp},i} - f_{\text{calc},i}|}{|f_{\text{exp},i}|}\right)\cdot 100\%,\ i = 1...N \quad (37)$$

where N, $f_{\text{exp},i}$, and $f_{\text{calc},i}$ are the sample number, measured and calculated parameters (void fraction or water velocity), respectively.
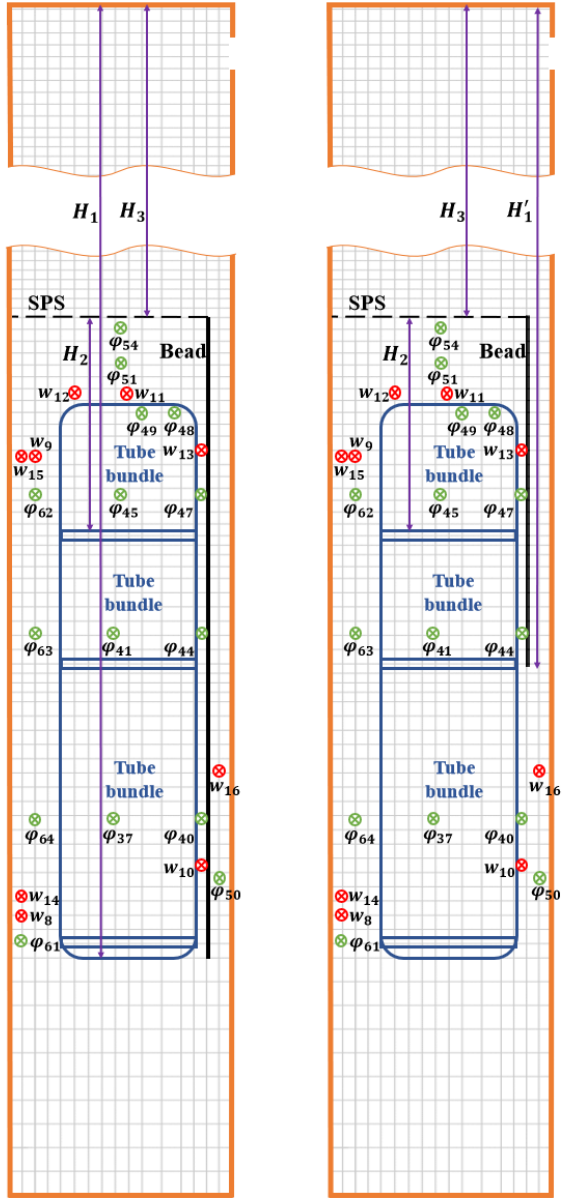
Figure 3: Nodalization scheme of the Model 1 (left) and Model 2 (right). Grid 16 × 124 φ_{37}, φ_{40}, ..., φ_{64} - void fraction sensors (green color); w_8, w_9, ..., w_{16} - velocity sensors (red color). (For interpretation of the references to color in this figure legend, the reader is referred to the web version of this article.)

MAD measures the average magnitude of the errors in a set of predictions, without considering their direction. MAXE defines a band within which there are deviations of the calculated values from the experimental ones, i.e. the uncertainty in the parameter prediction is ±MAXE.

Tables 6 and 7 summarize the deviations in the void fraction and water velocity predictions for all experimental series. For each test, N (sample number) is indicated, since in some tests not all sensors worked. The calculation errors
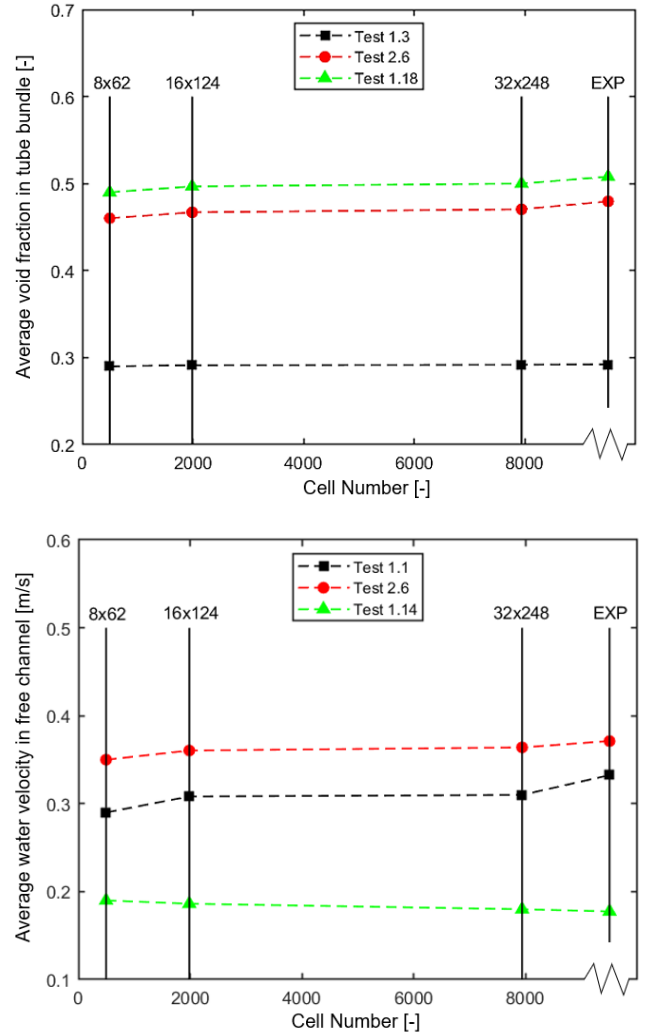
Figure 4: Grid independence check: (a) averaged void fraction in the tube bundle, (b) averaged velocity in the free channels. Experimental values (EXP) are also presented.
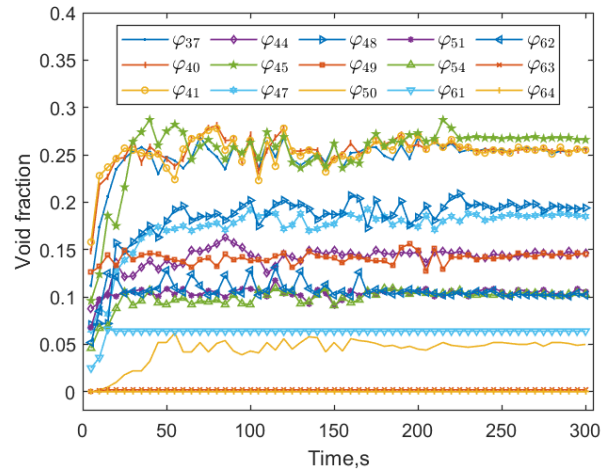
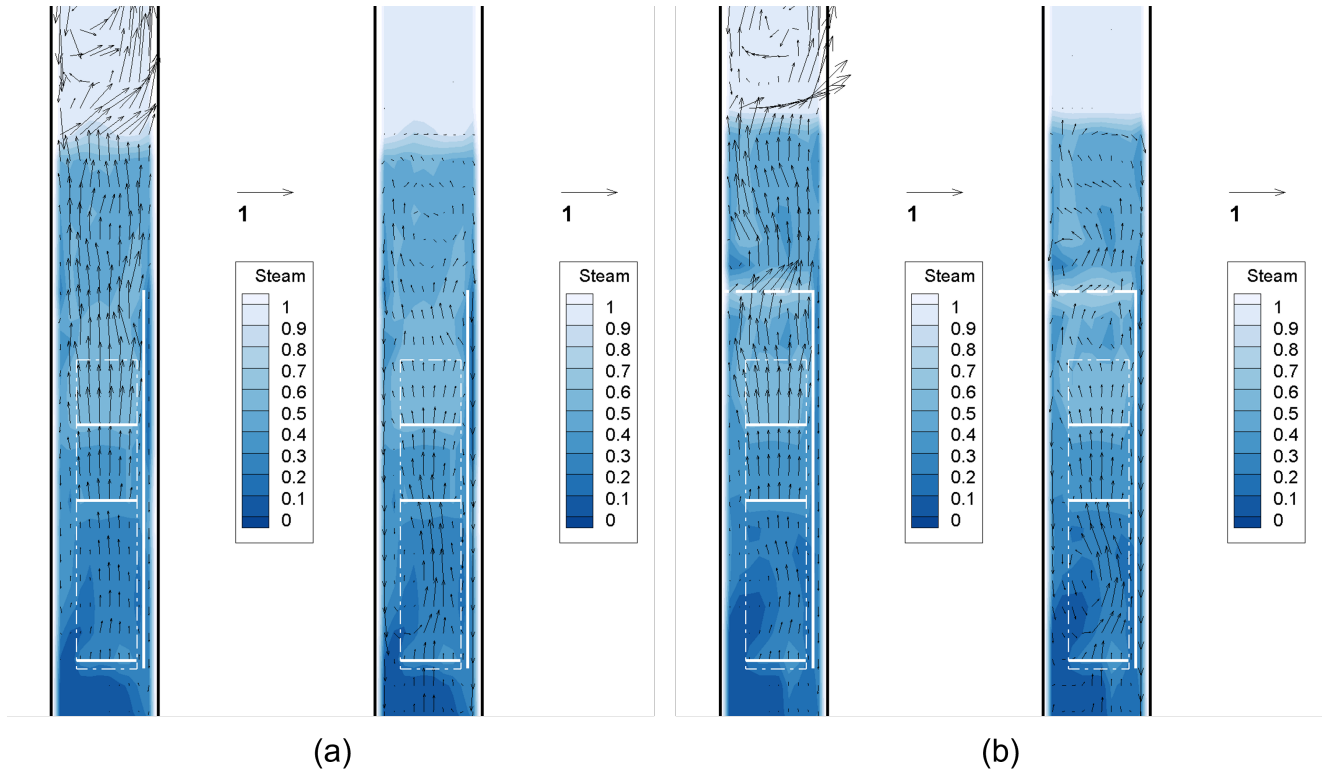**Figure 5:** The calculated void fractions vs time. Test 1.1. Grid 16 × 124.

Figure 6: Void fraction and superficial velocities of air (on the left) and water (on the right): (a) Test 1.6 (without SPS), total air superficial velocity 2.021 m/s; (b) Test 1.13 (SPS with perforation degree 4.5 %), total air superficial velocity 1.955 m/s.
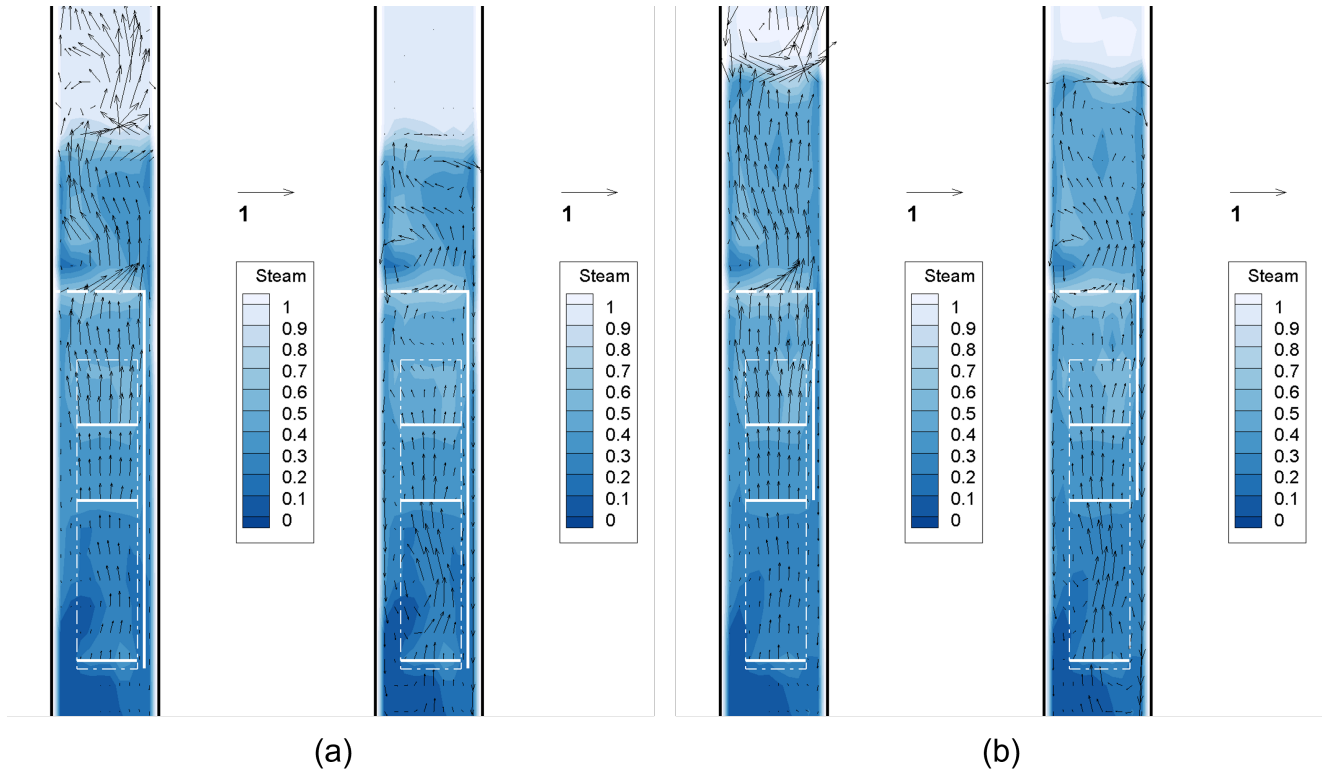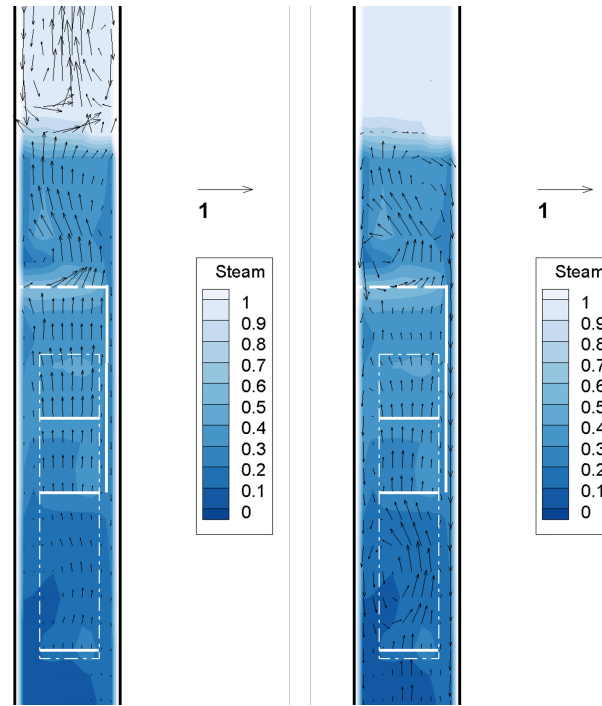

Figure 7: Void fraction and superficial velocities of air (on the left) and water (on the right). Tests with SPS perforation degree 7.5 %: (a) Test 1.17 (long bead), total air superficial velocity 1.670 m/s; (b) Test 2.11 (short bead), total air superficial velocity 1.688 m/s.

Figure 8: Void fraction and superficial velocities of air (on the left) and water (on the right). Test 2.13, SPS perforation degree 12 %, total air superficial velocity 1.141 m/s.

range as follows: 1) void fraction MAD = 1.57–13.27 % and MAXE = 3.31–55 %; 2) water velocity MAD = 1.72–10.49 %, MAXE = 2.78–40 %.

Table 6
MAD and MAXE in the void fraction and water velocity predictions. Model 1.

Test	Void fraction			Water velocity		
	N	MAD	MAXE	N	MAD	MAXE
Without SPS						
1.1	10	6.27%	15.20%	9	9.19%	30.00%
1.2	10	5.87%	11.43%	9	10.49%	40.00%
1.3	15	5.50%	12.50%	8	6.03%	16.32%
1.4	15	5.07%	15.74%	9	3.80%	7.22%
1.5	15	3.98%	20.89%	9	3.41%	8.06%
1.6	15	4.25%	15.48%	9	2.42%	8.33%
SPS with perforation degree 4.5%						
1.7	11	12.75%	24.73%	9	10.25%	31.67%
1.8	11	13.27%	55.00%	8	6.09%	13.16%
1.9	11	5.92%	18.57%	8	7.68%	22.08%
1.10	15	5.46%	13.61%	9	7.24%	19.17%
1.11	15	6.19%	17.81%	9	5.65%	11.67%
1.12	15	4.97%	28.57%	9	4.39%	8.75%
1.13	15	5.70%	24.00%	9	6.63%	17.14%
SPS with perforation degree 7.5%						
1.14	9	5.59%	17.44%	9	8.44%	15.45%
1.15	15	3.97%	13.60%	9	3.90%	7.77%
1.16	15	4.32%	26.50%	7	2.36%	3.92%
1.17	15	2.02%	8.39%	7	2.84%	4.21%
1.18	15	3.72%	11.04%	6	1.72%	2.78%

Fig. 13 presents a number of tests within different ranges of the MADs of void fractions and water velocities. Fig. 12(a) shows that the calculation errors of the 32 tests are <8%. Two tests have MADs of about 13%. It should be noted

Table 7
MAD and MAXE in the void fraction and water velocity predictions. Model 2.

Test	Void fraction			Water velocity		
	N	MAD	MAXE	N	MAD	MAXE
Without SPS						
2.1	11	5.05%	15.79%	9	4.51%	7.27%
2.2	11	5.12%	30.00%	9	2.48%	5.20%
2.3	11	3.09%	6.00%	9	5.72%	20.00%
2.4	11	2.70%	6.17%	9	5.17%	12.50%
2.5	11	1.57%	3.31%	9	3.66%	9.29%
SPS with perforation degree 4.5%						
2.6	15	3.55%	10.70%	9	5.67%	11.67%
2.7	15	5.75%	13.45%	4	5.09%	8.80%
SPS with perforation degree 7.5%						
2.8	11	3.51%	15.00%	9	4.11%	8.13%
2.9	15	3.34%	10.00%	9	2.74%	5.84%
2.10	15	3.11%	11.82%	9	3.35%	11.50%
2.11	15	3.07%	6.13%	9	3.51%	9.44%
2.12	15	2.36%	7.31%	9	2.19%	8.00%
SPS with perforation degree 12%						
2.13	11	4.38%	21.11%	9	2.27%	5.93%
2.14	11	2.53%	8.93%	9	2.53%	6.56%
2.15	11	3.42%	18.33%	9	2.13%	3.55%
2.16	11	1.93%	6.23%	9	3.23%	8.00%

that the largest errors in these two experiments are observed for void fraction values close to zero. For example, for Test 1.8 $\varphi_{50}^{exp} = 0.02$ and $\varphi_{50}^{calc} = 0.031$,
which gives absolute deviation according to the formula used in this paper AD = $|\varphi_{exp} - \varphi_{calc}|/\varphi_{exp} \cdot 100\%$ = $|0.02 - 0.031|/0.002 \cdot 100\% = 55\%$. If we use a weaker definition of the calculation error, which is also quite often used in
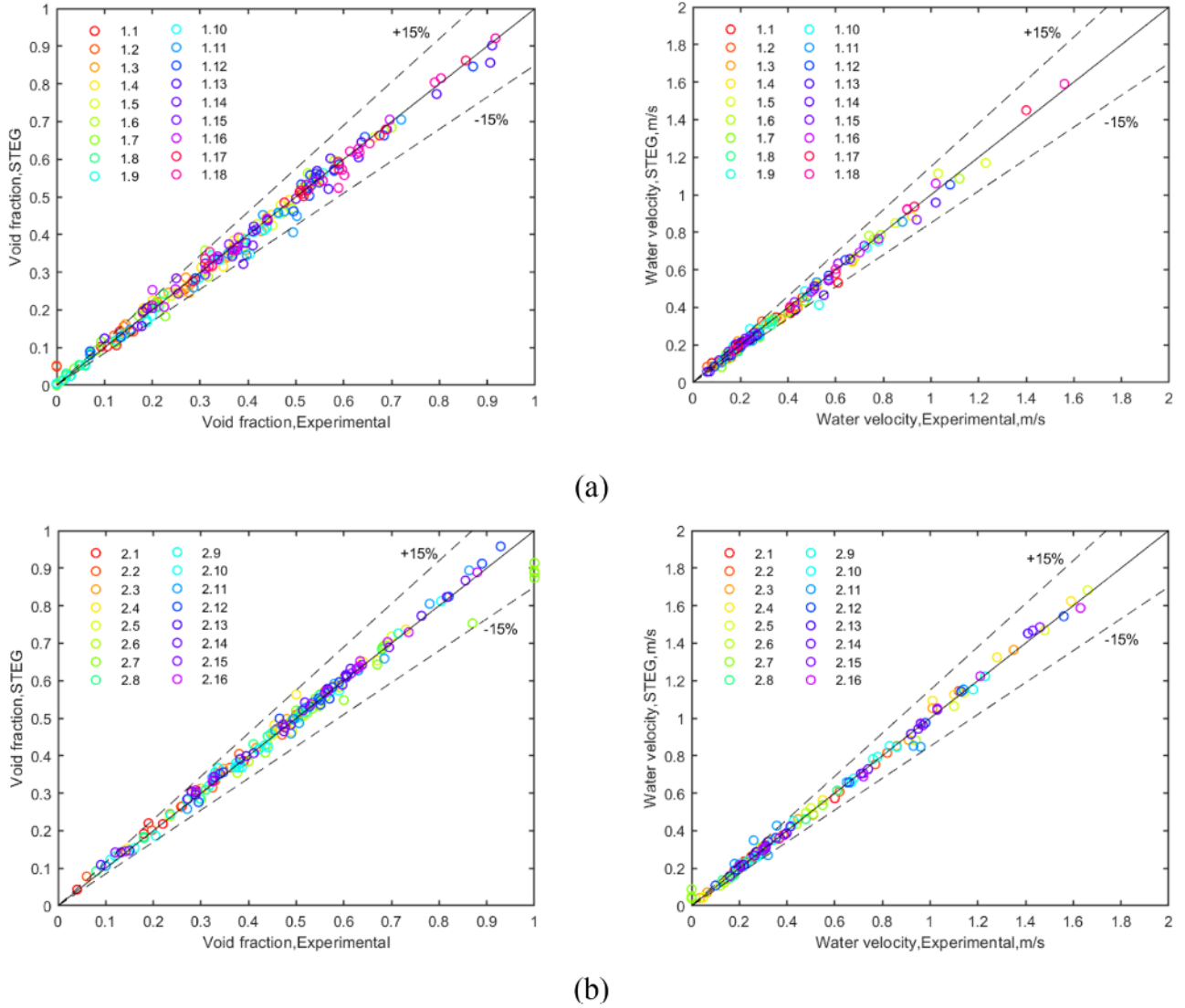
Figure 9: Comparison of the experimental data and the calculated values of the void fraction (on the left) and water velocities (on the right). (a) Model 1, (b) Model 2.

the literature, $\text{AD}_{\text{mod}} = |\varphi_{\text{exp}} - \varphi_{\text{calc}}| \cdot 100\%$. then for this measurement we obtain $\text{AD}_{\text{mod}} = |0.02 - 0.031| \cdot 100\% = 1.1\%$. However, in this paper, we have used the uniform definition of the calculation error for the void fraction and water velocity according to the formula (35). The predictions of water velocities are quite accurate: the MADs of 32 tests are <10 %, and all 34 MADs are less 12 %.

Fig. 14 presents a number of tests within different ranges of the ab- solute deviations (ADs) of void fractions and water velocities. A signif- icant number of experimental points is predicted by the STEG code with an error of <5%, for the void fraction of such points 311 (total number of points 442), i.e. 70% of the total number of points, and for the water velocity of such points 185 (total number of points 291), i.e. 64% of the total number of points. And a very large number of points (about 90% of the total number) both for the void fraction and for the water velocity are predicted by the STEG code with an accuracy of 10%. Recall that the measurement

error of these quantities is also estimated by experi- menters at 10%. It can be argued that the results generally indicate the relatively good predictive ability of the STEG code.

5. Summary and conclusions

The results of the validation of the STEG code using the experiments on two-phase air–water flow under typical conditions of a horizontal SG are presented. Two series of tests have been performed on Model 1 and Model 2, respectively. The main components of SG models are a stag- gered tube bundle, a submerged perforated sheet and a downcomer, which are placed in a transparent vessel. The geometrical characteristics of the tube bundle are taken as the full-scale WWER-1000 SG. The only difference between SG Models 1 and 2 is the height of the bead. Two SPSs with perforation degrees of 4.5% and 7.5% are used in Model 1, and three SPSs with perforation degrees of 4.5%, 7.5%
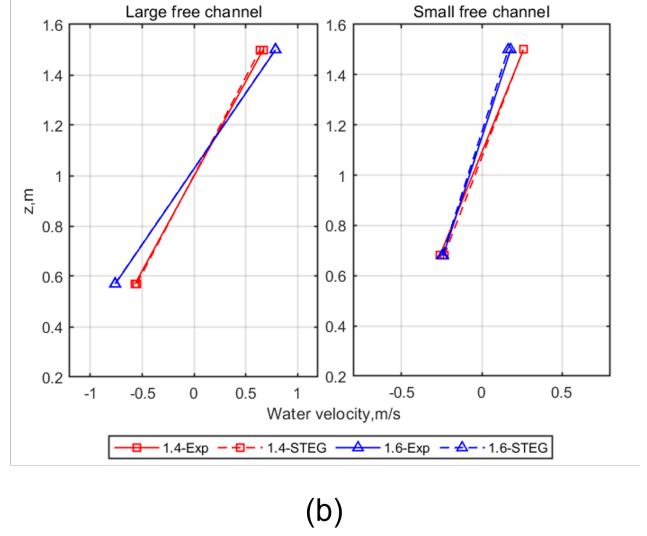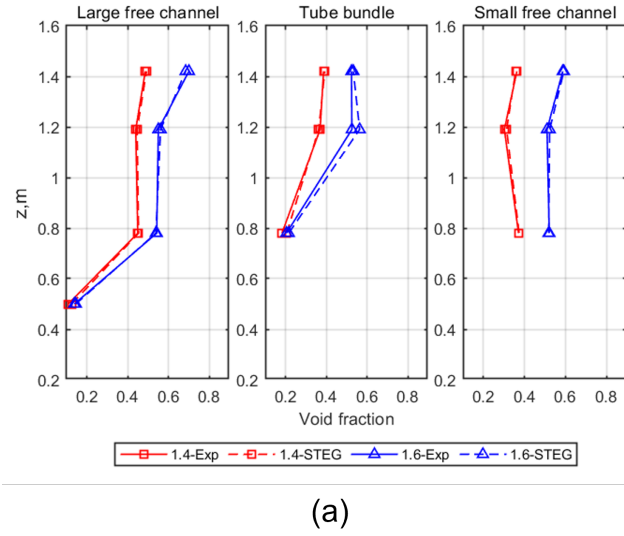
(a)

(b)

Figure 10: Comparison of calculated and experimental data, Model 1 (Tests 1.4 (red color)and 1.6 (blue color) without SPS): void fraction (a) and water velocity (b). (For interpretation of the references to color in this figure legend, the reader is referred to the web version of this article.)
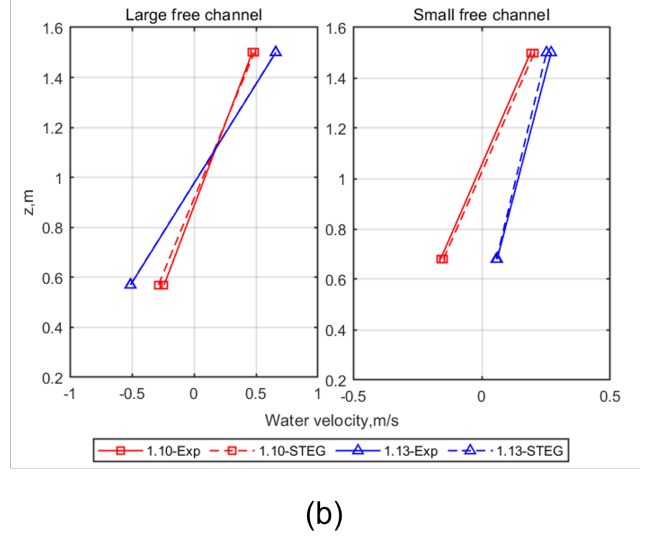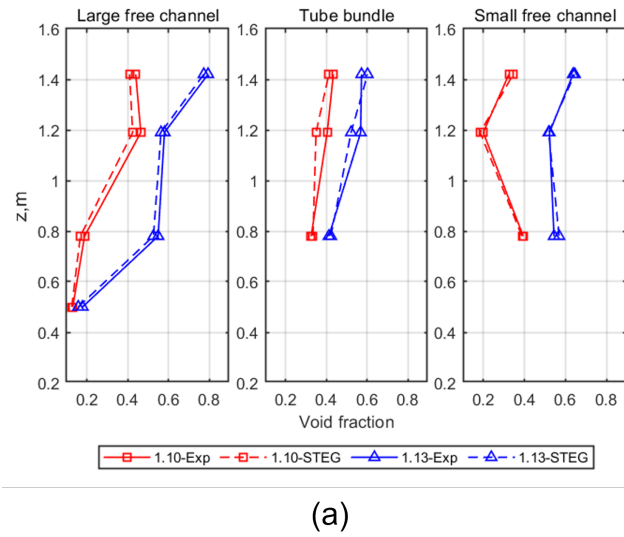

(a)

(b)

Figure 11: Comparison of calculated and experimental data, Model 1 (Tests 1.10 (red color) and 1.13 (blue color) with SPS 4.5%): void fraction (a) and water velocity (b). (For interpretation of the references to color in this figure legend, the reader is referred to the web version of this article.)

and 12% are used in Model 2. Also tests without SPS are performed. Air is supplied in three sections along the height of the tube bundle. The range of the superficial velocity of air is 0.07 – 2.0 m/s. The fifteen measurements of the void fraction and nine measurements of the water velocity are used. Each test is performed at a given air superficial velocity and water collapsed level. 18 tests on Model 1 and 16 tests on Model 2 have been performed. As a result of the investigations, 442 experimental points for the void fraction and 291 experimental points for the water velocity are obtained.

The STEG code is based on the 3D two-fluid model consisting of a system of mass and momentum conservation equations for the liquid and gas phases. In order to close the system of conservative equations, the laws of interface momentum transfer, the tube bundle, and the SPS flow resistance are defined.

All experiments are analyzed using the STEG code. The peculiarities of the spatial two-phase flows have been established, and a quantitative comparison with experimental data has been performed. The mean ab- solute deviations and maximum absolute errors of all 15 void fraction sensors and all 9 water velocity sensors are used as measures of the
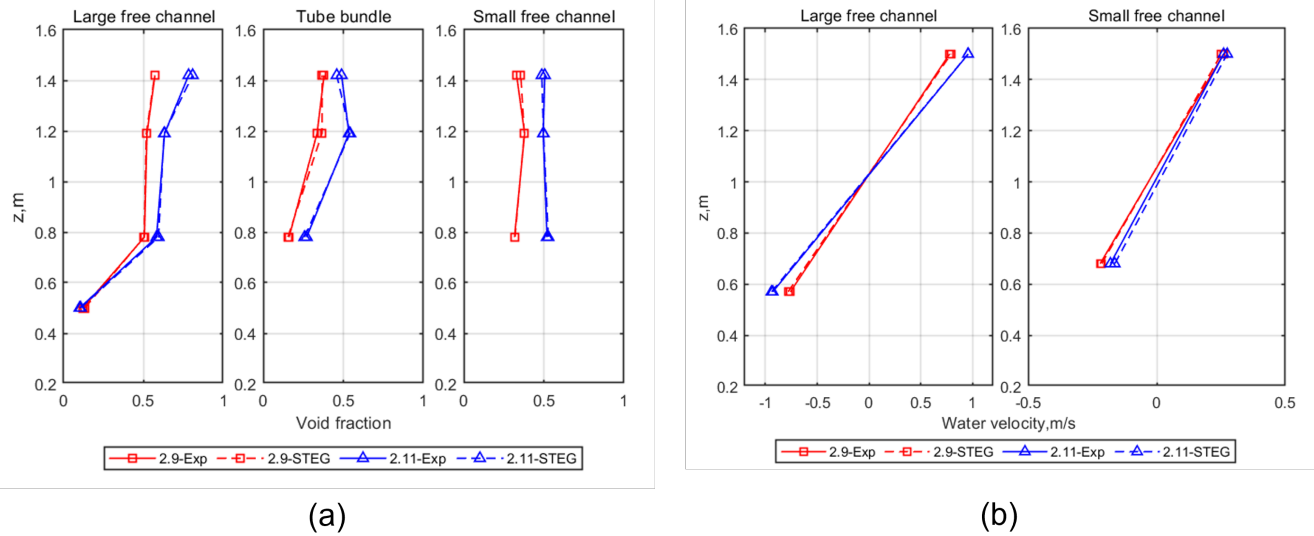
Figure 12: Comparison of calculated and experimental data, Model 2 (Tests 2.9 (red color) and 2.11 (blue color) with SPS 7.5%): void fraction (a) and water velocity (b). (For interpretation of the references to color in this figure legend, the reader is referred to the web version of this article.)
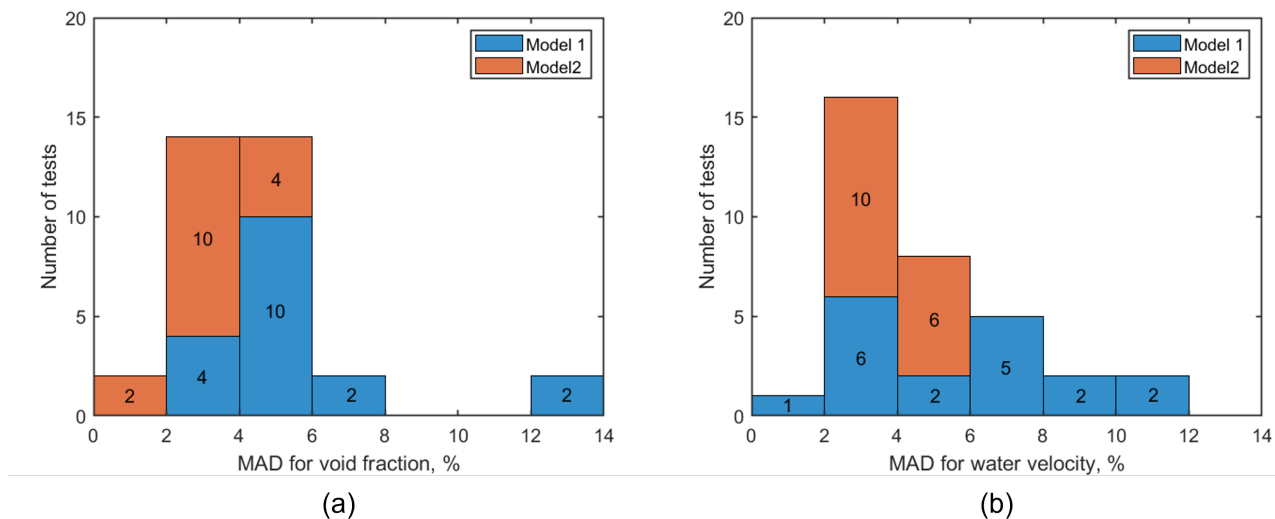

Figure 13: The number of tests within the corresponding ranges of MAD: (a) MAD of void fraction, (b) MAD of water velocity.

discrepancy between the experimental and calculated results for each test. The calculation errors range as follows: 1) void fraction MAD = 1.57–13.27% and MAXE = 3.31–55%; 2) water velocity MAD = 1.72–10.49%, MAXE = 2.78–40%. The MAD values of the void fraction for 32 out of 34 tests are <8%, the MAD values of water velocity for all 34 tests are <10.5%. Despite the fact that in some tests large MAXE values are observed, the number of points at which there are large de- viations of the calculated values from the experimental values is small. About 90% of all experimental points for the void fraction and water velocity are predicted by the STEG code with an accuracy of 10%, i.e. within the error of experimental measurement of these quantities.

Thus, to date, the STEG code has been validated on experimental data on the thermal hydraulics of horizontal steam generators obtained on PGV, PGV-1500 test facilities, on full-scale steam generator WWER- 1000 SG (Le et al, 2021b) and SG model (present work). Basic infor- mation about the experimental test facilities is given in Section 2 (see Table 3). The validation results are summarized in Table 8.

Most of the tests were performed on the PGV and SG model units - 44 and 34, respectively. For full-scale PG WWER-1000 SG, the data of only one experiment were analyzed. In general, it is evident that the STEG code can reasonably predict experimental data. Noteworthy is a rather
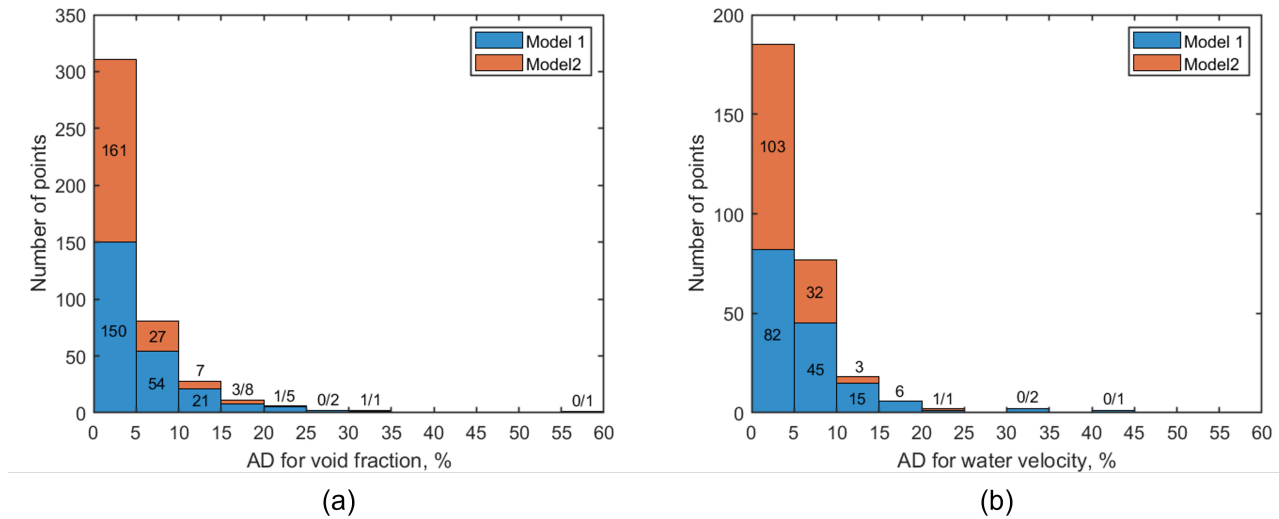
Figure 14: The number of data points within the corresponding ranges of AD: (a) AD of void fraction, (b) AD of water velocity.

Table 8
Results of the STEG code validation.

	Number of tests	Void fraction		Pressure difference		Water velocity	
		N	MAD	N	MAD	N	MAD
PGV	44	5	≤15%	4	≤40%	0	-
PGV-1500	4	15	≤6.5%	4	≤17%	0	-
WWER-1000 SG	16	5	≤3.3%	4	-	0	-
SG model	34	15	≤14%	4	-	0	≤12%

large discrepancy in the calculation of the pressure difference. This is due to the fact that in the experiments on the PGV test facility, both the regimes characteristic of the normal operation of a horizontal steam generator were studied, for which a fairly good agreement between the calculated pressure drops and the experiment (<20%) was obtained, and the regimes with highly uneven steam supply, where the discrepancies up to 40% in some cases (see Le et al., 2020b for details). In general, the results of the validation of experiments on the SG model (present work) correspond to the results of the validation carried out earlier.

References

[1] Ageev, A.G., Belov, V.I., Vasilyeva, R.V., 1988. Experimental and analytical study of limit loads under gravitational separation. In: Collection of scientific papers of Power Engineering Institute (ENIN), Moscow, 1988, pp.41–45 (In Russian).

[2] Ageev, A.G., Vasilyeva, R.V., Dmitriev, A.I., Tarankov, G.A., Titov, V.F., 1987. Investigation of hydrodynamics of steam generator PGV-1000. Elektricheskie Stancii (Power Stations) 6, 19–23 (In Russian).

[3] Blinkov, V.N., Elkin, I.V., Emelianov, D.A., et al., 2015. The influence of void fraction on the submerged perforated sheet hydraulic friction factor. Therm. Eng. 62, 484–489. https://doi.org/10.1134/S0040601515070010.

[4] Blinkov, V.N., Elkin, I.V., Emelianov, D.A., et al., 2016. Influence of non-uniformity of the submerged perforated sheet on steam demand leveling on the evaporation surface of a WWER steam generator. Therm. Eng. 63, 51–55. https://doi.org/10.1134/S0040601515120034.

[5] Ghazanfari, V., Ansarifar, G.R., Esteki, M.H., 2014. Drift flux modeling of the VVER-1000 horizontal nuclear steam generator. Prog. Nucl. Energy 76 (2014), 36–43. https:// doi.org/10.1016/j.pnucene.2014.04.021.

[6] Hovi, V., Ilvonen, M., 2010. PORFLO simulations of Loviisa horizontal steam generator. Research Report. No. VTT-R-01406-10. 18.2.2010.

[7] Idelchik, I.E., 1992. Hydraulic Resistance Handbook. Mashinostroenie, Moscow. In Russian.

[8] Ishii, M., Zuber, N., 1979. Drag coefficient and relative velocity in bubbly, droplet or particulate flows. AIChE J. 25 (5), 843–855. https://doi.org/10.1002/ aic.690250513.

[9] Kolbasnikov, A.V., 2000. Development of methods for calculation of the hydrodynamics of a two-phase medium and heat transfer in transversely flowed heating surfaces of steam generators on the basis of experimental studies. All-Russian Thermal Engineering Research Institute, Moscow. In Russian.

[10] Kolbasnikov, A.V., Shwartz, A.L., Galetsky, N.S., 1991. Investigation of steam-water hydrodynamics in immersed heating surfaces for improvement of steam generators of NPP with WWER. Power Technol. Eng. 8, 44–48. In Russian.

[11] Kolbasnikov, A.V., Shwartz, A.L., Galetsky, N.S., 1992. Investigation of two-phase hydrodynamics in immersed heating surfaces as applied to NPP steam generators. Therm. Eng. 4, 62–66. In Russian.

[12] Kroshilin, A.E., Kroshilin, V.E., Smirnov, A.V., 2008. Numerical investigation of threedimensional flows of steam-water mixture in the housing of the PGV-1000 steam generator. Therm. Eng. 55 (5), 372–379. https://doi.org/10.1134/ S0040601508050030.

[13] Le, T.T., Melikhov, V.I., Melikhov, O.I., Blinkov, V.N., Nerovnov, A.A., Nikonov, S.M., 2020a. Investigation of the equalization capability of submerged perforated sheets under thermal-hydraulic conditions of a horizontal steam generator. Ann. Nucl. Energy 148 (2020), 107715, 1-21. 10.1016/j.anucene.2020.107715.

[14] Le, T.T., Melikhov, V.I., Melikhov, O.I., Nerovnov, A.A., Nikonov, S.M., 2020b. Validation of the STEG code using PGV experiments on hydrodynamics of horizontal steam generator. Nucl. Eng. Des. 356 (2020) 110380, 1-18. https://doi.org/10.1016/j.nucengdes.2019.110380.

[15] Le, T.T., Melikhov, V.I., Melikhov, O.I., 2021a. Numerical analysis of the equalization capability of submerged perforated sheets for WWER-1500 horizontal steam generator. Ann. Nucl. Energy. Vol. 157 (2021), 108242, 1-14. https://www.scienc edirect.com/science/article/pii/S0306454921001183.

[16] Le, T.T., Melikhov, V.I., Melikhov, O.I., 2021b. Recommended set of interfacial drag correlations for the two-phase flow under thermal-hydraulic conditions of a horizontal steam generator. Nucl. Eng. Des. 379 (2021), 111249, 1-20. https://doi.org/10.1016/j.nucengdes.2021.111249.

[17] Liles, D.R., Reed, W.H., 1978. A semi-implicit method for two-phase fluid dynamics. J. Comp. Phys. 26, 390–407. https://doi.org/10.1016/0021-9991(78)90077-3.

[18] Lukasevich, B.I., Trunov, N.B., Dragunov, Y.G., Davidenko, S.E., 2004. Steam Generators of VVER Reactors for Nuclear Power Plants. Akademkniga, Moscow. In Russian.

[19] Maslovaric, B., Prica, S., Stevanovic, V., Stosic, Z., 2004. CFD simulation of steam generator tube rupture thermal-hydraulics. Proc. 12th Int. Conf. Nucl. Eng., ICONE12-49403, April 25-29, 2004 Arlington, Virginia USA.

[20] Melikhov, O.I., Melikhov, V.I., Nikonov, S.M. et al. 2015b, Validation and improvement of the STEG code on the basis of the experimental data, obtained at PGV test facility. Calculation analysis of the tests at the PGV test facility. Transactions of the 9th International Scientific and Technical Conference "Safety Assurance of NPP with WWER", May 19-22, 2015, OKB "GIDROPRESS", Podolsk, Russia. http://www.gidro press.podolsk.ru/files/proceedings/mntk2015/autorun/article144-en.htm.

[21] Melikhov, V.I., Melikhov, O.I., Nigmatulin, B.I., 1995a. Numerical modeling of secondary side thermalhydraulics of horizontal steam generator. Proc. 3rd Int. Seminar on Horizontal Steam Generators, pp.249-270, Lappeenranta, Finland.

[22] Melikhov, V.I., Melikhov, O.I., Nigmatulin, B.I., 1995b. Mathematical modelling of horizontal steam generator. Proc. 2nd Int. Conf. Multiphase Flow, Vol.4, P8-9 - P815, April 3-7, 1995, Kyoto, Japan.

[23] Melikhov, V.I., Melikhov, O.I., Nigmatulin, B.I., 1995c. Thermalhydraulic analysis of horizontal steam generator. Proc. First Int. Symp. Two-Phase Flow Modelling and Experimentation, Vol.1, pp.511-518, 9-11 October, 1995, Rome, Italy.

[24] Melikhov, O.I., Elkin, I.V., Melikhov, V.I., Nikonov, S.M., et al., 2015a, Experimental researches of hydraulic resistance and leveling capacity of the submerged perforated sheet in PGV test facility (EREC). Transactions of the 9th International Scientific and Technical Conference "Safety Assurance of NPP with WWER", May 19-22, 2015, OKB "GIDROPRESS", Podolsk, Russia. http://www.gidropress.podolsk.ru/files/proceedings/mntk2015/autorun/article143-en.htm.

[25] Melikhov, V.I., Melikhov, O.I., Nerovnov, A.A., Nikonov, S.M., 2018. An investigation into the behavior of a steam-water mixture flow through holes in a submerged perforated sheet at high void fractions. Therm. Eng. 65, 45–50. https://doi.org/10.1134/S0040601518010032.

[26] Ohnuki, A., Akimoto, H., 2000. Experimental study on transition of flow pattern and phase distribution in upward air-water two-phase flow along a large vertical pipe. Int. J. Multiphase Flow 26 (2000), 367–386. https://doi.org/10.1016/S0301-9322%2899%2900024-5.

[27] Ozar, B., Dixit, A., Chen, S.W., Hibiki, T., Ishii, M., 2012. Interfacial area concentration in gas-liquid bubbly to churn-turbulent flow regime. Int. J. Heat and Fluid Flow 38 (2012), 168–179. https://doi.org/10.1016/j.ijheatfluidflow.2012.08.006.

[28] Papp L., Vacek J., 2017. WWER steam generators. In: Steam Generators for Nuclear Power Plants. Ed. J. Rizic., 1st Edition, Woodhead Publishing Series in Energy. P. 107-124. https://doi.org/10.1016/C2015-0-01340-5.

[29] Rabiee, A., Kamalinia, A.H., Haddad, K., 2016. Horizontal steam generator thermal hydraulic simulation in typical steady and transient conditions. Nucl. Eng. Des. 305 (2016), 465–475.

https://doi.org/10.1016/j.nucengdes.2016.06.004.

[30] Rabiee, A., Kamalinia, A.H., Haddad, K., 2017. Two-phase flow field simulation of horizontal steam generators. Nucl. Eng. Technol. 49 (1), 92–102. https://doi.org/ 10.1016/j.net.2016.08.008.

[31] RELAP5/Mod3.3, 2001. Code Manual, Volume IV: Models and Correlations, NUREG/CR5535, Vol. IV.

[32] Rousseau, J.C., Houdayer, G., 1983. Advanced safety code CATHARE summary of verification studies on separate effects experiments. In: Proceedings of the Second International Topical Meeting on Nuclear Reactor Thermalhydraulics. Santa Barbara, CA.

[33] Ryabov, G.A., Karasev, V.B., Kozlov, Y.V., 1984. Experimental investigation of hydraulic resistance of perforated sheets using steam-water mixture. Therm. Eng. 6, 68–70 in Russian.

[34] Safavi, A., Abdi, M.R., Aghaie, M., Esteki, M.H., Zolfaghair, A., Pilevar, A.F., Daryabak, A., 2013. Study of perforated plate effect in horizontal WWER-1000 steam generator. Nucl. Eng. Des. 256 (2013), 249–255.

[35] Schlegel, J.P., Hibiki, T., 2015. A correlation for interfacial area concentration in high void fraction flows in large diameter channels. Chem. Eng. Sci. 131 (2015), 172–186. https://doi.org/10.1016/j.ces.2015.04.004.

[36] Schlegel, J.P., Sawant, P., Paranjape, S., Ozar, B., Hibiki, T., Ishii, M., 2009. Void fraction and flow regime in adiabatic upward two-phase flow in large diameter vertical pipes. Nucl. Eng. Des. 239 (2009), 2864–2874. https://doi.org/10.1016/j. nucengdes.2009.08.004.

[37] Shen, X., Schlegel, J.P., Chen, S. Rassame, S., Griffiths, M.J., Hibiki, T., Ishii, M., 2014. Flow Characteristics and Void Fraction Prediction in Large Diameter Pipes. Frontiers and Progress in Multiphase Flow I, Chapter 2. Springer, New York. https://doi.org/10.1007/978-3-319-04358-6_2.

[38] Simovic, Z.R., Ocokoljic, S., Stefanovic, V.D., 2007. Interfacial friction correlations for the two-phase flow across tube bundles. Int. J. Multiphase Flow. 33 (2), 217–226. https://doi.org/10.1016/j.ijmultiphaseflow.2006.08.003.

[39] Stevanovic, V.D., Stosic, Z.V., Kiera, M., 2002a. Horizontal steam generator thermalhydraulics at various stead-state power levels. Proc. ICONE10, ICONE10-22451, 10th Int. Conf. Nucl. Eng., April 14-18, 2002, Arlington, VA.

[40] Stevanovic, V.D., Stosic, Z.V., Kiera, M., Stoll, U., 2002b. Numerical simulation and analyses of the loss of feedwater transient at the Unit 4 of KOLA NPP. Proc. ICONE10, ICONE10-22452, 10th Int. Conf. Nucl. Eng., April 14-18, 2002, Arlington, VA.

[41] Stosic, Z.V., Stevanovic, V.D., 2002. Advanced three-dimensional two-fluid porous media method for transient two-phase flow thermal-hydraulics in complex geometries. Numer. Heat Transf. Part B 41 (3–4), 263–289. https://doi.org/10.1080/ 104077902753541014.

[42] TRAC–PF1/MOD2., 1990. Theory Manual. Los Alamos National Laboratory. November 1990. Los Alamos. NM 87545.

[43] Trunov, N.B., Logvinov, S.A., Dragunov, Y.G., 2001. Hydrodynamics and ThermoMechanical Processes in the Steam Generators of NPP with WWER. Energoatomizdat, Moscow. In Russian.

[44] Wallis, G.B., 1969. One-Dimensional Two-Phase Flow. McGraw-Hill, New York.

[45] Zarifi, E., Jahanfarnia, G.R., Mousavian, S.K., D'Auria, F., 2009. Semi 2D modeling of the horizontal steam generator PGV-1000 using the RELAP5 code. Prog. Nucl. Energy 51 (2009), 788–798.